Rab29 knock-out or transgenic overexpression does not impact basal LRRK2 activity in wildtype and pathogenic mouse and cell line models

Alexia F. Kalogeropulou[1], Pawel Lis[1], Nicole K. Polinski[2], Dario R. Alessi[1]
1 Medical Research Council (MRC) Protein Phosphorylation and Ubiquitylation Unit, School of Life Sciences, University of Dundee, Dow Street, Dundee DD1 5EH, UK

2 Michael J Fox Foundation for Parkinson's Research Grand Central Station, PO Box 4777, New York, NY 10163, U.S.A.

*Correspondence to Alexia F. Kalogeropulou (a.kalogeropulou@dundee.ac.uk) or Dario R Alessi (d.r.alessi@dundee.ac.uk)

Abstract
Mutations that enhance LRRK2 protein kinase activity cause inherited Parkinson's disease. LRRK2 phosphorylates a group of Rab GTPase proteins, including Rab10, within the effector-binding switch-II motif. Previous work has indicated that the PARK16 locus, which harbors the gene encoding for Rab29, is mutated in Parkinson's, and that Rab29 operates in a common pathway with LRRK2. Co-expression of Rab29 and LRRK2 stimulates LRRK2 activity by recruiting LRRK2 to the surface of the trans-Golgi network. Pathogenic mutations including LRRK2[R1441C] promote GTP-binding are more readily activated by Rab29. As previous work was based on overexpression approaches, we were curious to define the importance of endogenous Rab29 in regulating basal LRRK2 activity. We report that knock-out of Rab29 does not influence endogenous LRRK2 activity, based on assessment of Rab10 phosphorylation, in wildtype LRRK2, LRRK2[R1441C] as well as in VPS35[D620N] knock-in mouse tissues and embryonic fibroblasts. We also generated a transgenic mouse model that moderately overexpresses Rab29, and found that this was not sufficient to stimulate basal LRRK2 activity. Our data suggest that the bulk of the basal LRRK2 activity measured in whole cell and tissue extracts is not controlled by Rab29. LRRK2 is not associated with the Golgi unless Rab29 is highly overexpressed, which could account for the lack of effect that Rab29 knock-out or moderate overexpression has on basal LRRK2 activity. Further work is required to establish how basal LRRK2 activity is regulated, and whether other Rab proteins control basal LRRK2 by targeting it to diverse membranes.

Introduction
Autosomal dominant missense mutations that hyperactivate LRRK2 (leucine rich repeat kinase 2), are one of the most common causes of familial Parkinson's disease (PD) [1–4]. Age of onset and progression of LRRK2-driven PD is virtually indistinguishable from sporadic PD, which comprises the vast majority of the patient population. LRRK2 is a large, multi-functional protein kinase that encodes two central catalytic regions, a Roc-type GTPase domain adjacent to a COR (C-terminal of Roc) domain, which is followed by a serine/threonine protein kinase domain. These enzymatic regions are surrounded by several domains, including N-terminal armadillo and ankyrin domains, leucine-rich repeats and a C-terminal WD-40 repeat [5]. The most prevalent LRRK2 pathogenic variants map to either the GTPase Roc [N1437H, R1441C/G/H] or COR [Y1699C] domains, or the kinase domain [G2019S, I2020T], and act as gain-of-function mutations by enhancing LRRK2 kinase activity [6–10]. The mutations within the GTPase Roc/COR domain are proposed to inhibit GTPase

activity and enhance GTP binding [11–13]. The mutations within the GTPase domain do not directly activate LRRK2 activity *in vitro*, but enhance interaction with Rab29 located at the Golgi [14,15]. This leads to the recruitment of LRRK2 to the Golgi membrane surface which enhances kinase activity, as evidenced through increased autophosphorylation at Ser1292 and phosphorylation of its physiological Rab protein substrates, through a yet undefined mechanism [14,16,17]. The mutations within the kinase domain directly stimulate LRRK2 activity by promoting a more closed active conformation of the catalytic moiety [18–20]. Recent work has also revealed that the VPS35[D620N] autosomal dominant mutation that causes PD markedly elevates Rab protein phosphorylation by LRRK2 through an unknown mechanism [21]. LRRK2 is constitutively phosphorylated on several well studied serine residues in its N-terminus, specifically Ser910, Ser935, Ser955, and Ser973, and these sites are rapidly dephosphorylated upon pharmacological inhibition of LRRK2 [22,23]. LRRK2 protein kinase inhibitors are currently in early stage clinical trials for LRRK2-driven PD [24,25].

Well-characterized and validated substrates of LRRK2 comprise a subset of Rab GTPases that include Rab8A, Rab10, Rab12 and Rab29 [7,26]. Rab GTPases are crucial regulators of intracellular vesicle trafficking, implicated in vesicle formation and transport between target membranes in a tightly controlled network [27]. They influence biology by interacting with a series of effector proteins when complexed to GTP. LRRK2 phosphorylates Rab proteins at a highly conserved Ser/Thr residue located at the center of the effector binding region of these enzymes that is also known as the Switch-II motif [7,26,28]. This phosphorylation event appears to act in two ways. Firstly, it prevents Rab proteins interacting with many of their known interactors including guanine nucleotide exchange factors (GEFs) and guanine dissociation inhibitors (GDIs) that are required for the shuttling of Rab proteins between membrane compartments. This results in the LRRK2-phosphorylated Rab proteins accumulating within the compartment that they are phosphorylated [7,29]. Secondly, LRRK2-phosphorylated Rab8A and Rab10 bind preferentially to a set of effectors such as RILPL1 and RILPL2 which are implicated in ciliogenesis [26]. These possess a RH2 domain that functions as a phospho-Rab recognition domain [30]. Pathogenic LRRK2 mutants decrease primary cilia formation in cell culture in a manner that is rescued upon LRRK2 inhibition [26]. The ability of LRRK2 to inhibit ciliogenesis requires RILPL1 binding to LRRK2-phosphorylated Rab8A and Rab10 [31,32].

Significant effort has focused on Rab29, also known as Rab7L1, and its possible roles in regulating LRRK2. The gene encoding Rab29 lies within a genetically complex locus termed PARK16 implicated with increased PD risk [33–36]. The PARK16 locus contains 5 genes, and it is not clear which of these genes are relevant for PD or how the numerous variants identified within this locus affect gene expression and/or function. Single nucleotide polymorphisms in non-coding regions of the PARK16 locus have been linked to increasing the transcriptional regulation of Rab29 mRNA [15,37,38]. To our knowledge, PARK16 variants linked with PD have not been shown to increase Rab29 protein expression. Several earlier studies alluded to the possibility of Rab29 and LRRK2 acting in converging pathways, by demonstrating epistatic interactions between polymorphisms in the LRRK2 and Rab29 genes that increase PD risk [38,39]. Physical interaction between LRRK2 and Rab29, either *in vitro* or based on a co- immunoprecipitation analysis, has also been demonstrated [15,38,40,41]. Furthermore, analysis of genetic models demonstrates that Rab29 and LRRK2

operate coordinately to control axon elongation in *C. elegans,* and lysosomal trafficking and kidney pathology in mice [42]. A recent study reports that combined knock-out of LRRK2 and Rab29 does not result in a PD-relevant neuronal pathology or behavioral abnormalities [43]. Rab29 has been implicated in maintaining Golgi morphology and in mediating the retrograde trafficking of the mannose6-phosphate receptor (M6PR), which recognizes and sorts lysosomal enzymes from the trans-Golgi to late endosomes and lysosomes [44,45]. An intriguing finding that implicates Rab29 in immune response demonstrated Rab29 recruitment to *S. typhi*-containing vacuoles and Rab29 involvement in the generation of typhoid toxin transport intermediates that release the toxin into the extracellular environment [46].

Rab29 belongs to a subfamily of Rab GTPases with Rab32 and Rab38, which are localized to the melanosome and are involved in regulating the trafficking of melanogenic enzymes between the *trans*-Golgi and melanosomes [47]. Rab29 is unique among the Rab proteins targeted by LRRK2, in that it possesses two adjacent phosphorylated residues within its Switch-II motif, namely Thr71 and Ser72. Ser72 aligns with the phosphorylation site found in other LRRK2 substrates. To our knowledge there is no evidence that endogenous Rab29 is directly phosphorylated by LRRK2, but in overexpression studies LRRK2 triggers phosphorylation of both Thr71 and Ser72 in a manner that is blocked with LRRK2 inhibitors [14,26]. Based on mutagenesis overexpression experiments, phosphorylation of these sites on Rab29 was proposed to function as a negative feedback loop to block activation of LRRK2 by Rab29 [14]. Rab32 and Rab38 are not phosphorylated by LRRK2 and do not possess a Ser/Thr residue at the equivalent position within their switch-II motif [26]. Recent work has established that the activation of LRRK2 by Rab29 occurs irrespective of the identity of the membrane to which Rab29 is attached [29], and requires prenylation and nucleotide binding of LRRK2 and Rab29 [16,29]. The numerous genetic studies in addition to data presented *in vitro,* in cells, and in model organisms, provide substantial evidence that LRRK2 and Rab29 pathways intersect.

The previous work showing that LRRK2 is activated by being recruited to the Golgi via interaction with Rab29 is largely based in overexpression experiments in which both Rab29 and wildtype or pathogenic mutants of LRRK2 are co-expressed. In this study, we sought to investigate the physiological relevance of Rab29 as a regulator of endogenous LRRK2 in cell lines as well as mouse tissues. We describe our efforts to thoroughly characterize four different mouse models that we generated to assess Rab29 impact on basal activity of wildtype and the LRRK2[R1441C] pathogenic mutant. Our data demonstrate that knock-out or moderate transgenic overexpression of Rab29 in a new mouse model we created, does not significantly impact the ability of LRRK2 to phosphorylate Rab10 or Rab12. Furthermore, we show that knock-out of Rab29 does not impact the ability of the VPS35[D620N] mutation to promote Rab10 protein phosphorylation. Our data indicate that Rab29 is not a major regulator of basal wildtype or LRRK2[R1441C] activity measured in whole cell or tissue extracts that we have analyzed.

Materials and Methods

Reagents

MLi-2 LRRK2 inhibitor was synthesized by Natalia Shpiro (University of Dundee) and was first described to be a selective LRRK2 inhibitor in previous work [48]. Microcystin-LR was purchased from Enzo Life Sciences (ALX-350-012). Oriole fluorescent gel stain was purchased from Bio-Rad (#161-0495).

Generation of MJFF rabbit monoclonal Rab29 total antibodies (MJF-30)

Rabbit immunization and rabbit antibody generation was performed by Abcam Inc. (Burlingame, CA). To generate the Rab29 total antibodies, full length recombinant proteins as well as N-terminal and C-terminal peptides were used. Abcam performed three subcutaneous injections using the immunogens conjugated with KLH, followed by two subcutaneous injections using the immunogens conjugated with ovalbumin. Target immunogen is described in Table 1. Following the initial injections with full-length proteins, booster immunizations using N-terminal and C-terminal peptides were performed. The provided bleeds (1 pre-immunization, 2 bleeds after immunization with full-length protein, 1 bleed after additional immunization with the N- and C-terminal peptides) from immunized animals (6 rabbits – E8767-E8772) were tested at 1:1000 dilution using lysates of A549 wildtype and Rab29 knock-out cell lysates. Rabbits producing the best antibody were chosen for monoclonal antibody generation. Hybridoma fusion was performed according to an established protocol [49]. Abcam used a process omitting the multi-clone stage, and provided 81 single clones directly. Single-clone supernatants were screened using immunoblots of A549 wildtype and Rab29 knock-out cell lysates. The top eight clones which gave the most robust signal were additionally tested using MEF lysates to check for human/mouse Rab29 specificity. Clone #124 was able to detect both human and mouse Rab29, while clone #104, which only detected human Rab29, showed the strongest and cleanest signal. Based on these results, clones #104 (human selective catalogue number ab256527) and clone #124 (human + mouse selective antibody catalogue number ab256526) were chosen for recombinant antibody generation and are now available commercially from Abcam.

Other Antibodies

The MJFF rabbit monoclonal antibody Rab10 pThr73 was previously characterized [50], and purchased through Abcam (ab230261) and used at 1:1000. The MJFF rabbit monoclonal Rab12 pSer105 (equivalent phosphorylation site to human pSer106) antibody was described previously [21], and is available from Abcam (ab256487). The mouse monoclonal antibody against total LRRK2 (C-terminus) was from NeuroMab (clone N241A/34, #75-253) and diluted 1:1000. Rabbit monoclonal anti-Rab10 (#8127), and mouse monoclonal alpha-tubulin (#3873) were from Cell Signaling Technology and used at 1:1000. Mouse monoclonal Rab32 (B-4) antibody was from Santa Cruz Biotechnology (sc-390178) and was diluted 1:200. The mouse monoclonal anti-Rab10 total antibody was from Nanotools (#0680–100/Rab10-605B11) and used at a final concentration of 1 μg/ml. Mouse anti-glyceraldehyde-3-phosphate dehydrogenase (GAPDH) was from Santa Cruz Biotechnology (sc-32233) and was used at 1:2000. Rabbit monoclonal antibodies for total LRRK2 (N-terminus) (UDD3) and pSer935 LRRK2 (UDD2), and sheep polyclonal antibodies Rab29 total (S984D) and Rab12 total (SA227) were purified by MRC-PPU Reagents and Services at the University of Dundee and were all used at a final concentration of 1 μg/ml. All rabbit and

mouse primary antibodies were diluted in 5% (w/v) bovine serum albumin (BSA) dissolved in TBS-T (50 mM Tris base, 150 mM sodium chloride (NaCl), 0.1% (v/v) Tween 20). Sheep polyclonal antibodies were diluted in 5% (w/v) milk dissolved in TBS-T. Goat anti-mouse IRDye 800CW (#926-32210), goat anti-mouse IRDye 680LT (#926-68020), goat anti-rabbit IRDye 800CW (#926-32211), and donkey anti-goat IRDye 800CW (#926-32214) IgG (H+L) secondary antibodies were from LI-COR and were diluted 1:10000 in 5% (w/v) milk in TBS-T.

Mice

Mice selected for this study were maintained under specific pathogen-free conditions at the University of Dundee (UK). All animal studies were ethically reviewed and carried out in accordance with Animals (Scientific Procedures) Act 1986 and regulations set by the University of Dundee and the U.K. Home Office. Animal studies and breeding were approved by the University of Dundee ethical committee and performed under a U.K. Home Office project license. Mice were housed at an ambient temperature (20–24°C) and humidity (45–55%) and were maintained on a 12 h light/12 h dark cycle, with free access to food (SDS RM No. 3 autoclavable) and water. For the experiments described in Fig 2B-D and Fig S1 (Rab29 knock-out model), Fig 4A-F (transgenic Rab29 overexpression model), Fig 5B-D and Fig S4 (Rab29 knock-out LRRK2[R1441C] knock-in model), and Fig 6B-D and Fig S5 (Rab29 knock-out VPS35[D620N] knock-in model), 6-month-old littermate matched or matched mice of the indicated genotypes were injected subcutaneously with vehicle [40% (w/v) (2-hydroxypropyl)-β-cyclodextrin (Sigma–Aldrich #332607)] or MLi-2 dissolved in vehicle at a 30mg/kg final dose. Mice were killed by cervical dislocation 2 hours following treatment and the collected tissues were rapidly snap-frozen in liquid nitrogen. For the experiment outlined in Fig S2 (transgenic Rab29 overexpression model), mice ranging from 3 to 4 months of the indicated genotypes were dosed, killed and tissues were isolated as outlined above. For the studies involving 18-24 mice which took place over multiple days, the genotypes and treatments were randomized each day to account for any temporal differences, such as light and ventilation. A general overview of the mouse models utilized in this study is outlined in Table 2.

Generation of Rab29 knock-out mice

Rab29 knock-out mice are made available through the Wellcome Trust Sanger Institute and distributed by Infrafrontier: EMMA mouse repository (EM: 05517), and were characterized previously [42]. LacZ-knock-in Rab29$^{tm1a(EUCOMM)Wtsi}$ mice were bred with Taconic Total Body Cre mice expressing Cre recombinase (Model 12524), which recognizes the loxP sites that flank the inserted promoter-driven neomycin cassette and exon 4 of Rab29, which is critical for expression. Following the deletion of exon 4, the mice were then bred and maintained on a C57Bl/6j background to remove the Cre recombinase allele, and to produce the experimental animals used in this study. The genotypes of the Rab29 knock-out mice were confirmed by PCR using genomic DNA isolated from ear biopsies and primers that amplify the entire Rab29 gene, as well as by immunoblotting.

Generation of Rab29-Knock-out LRRK2[R1441C] and Rab29-Knock-out VPS35[D620N] knock-in mice

The generation of LRRK2[R1441C] knock-in mice and VPS35[D620N] knock-in mice were described previously [21,26]. Rab29 knock-out heterozygous mice were crossed with LRRK2[R1441C] or VPS35[D620N] knock-in homozygous mice to produce double

heterozygous mice for Rab29 knock-out and LRRK2[R1441C] or VPS35[D620N] knock-in. Double heterozygous mice were crossed to produce the following genotypes: Rab29 wildtype/LRRK2 (or VPS35) wildtype, Rab29 knock-out/LRRK2 (or VPS35) wildtype, Rab29 wildtype/LRRK2[R1441C] (or VPS35[D620N]), or Rab29 knock-out/LRRK2[R1441C] (or VPS35[D620N]) (1/16 frequency of indicated genotypes by Mendelian inheritance). Double homozygous mice of the aforementioned genotypes were then expanded as four different subsets to produce additional double homozygous mice for mouse embryonic fibroblast generation and MLi-2 injection studies. Matched mice of the same generation were used for experimental studies.

Generation of transgenic Rab29 overexpressing mice

The Michael J. Fox Foundation for Parkinson's Research generated the transgenic Rab29-overexpressing mouse model (C57BL/6NTac-Gt(ROSA)26Sortm1(Pgk-Rab29)Tac), which is made available through Taconic (Model 16552). The constitutive knock-in of Pgk-Rab29 in the ROSA26 locus via targeted transgenesis was undertaken by Taconic. The Rab29 sequence was synthesized according to the NCBI transcript NM_144875.2. The following elements were inserted into the ROSA26 locus (NCBI gene ID: 14910) using Recombination-Mediated Cassette Exchange (RMCE): a Pgk promoter, the Rab29 open reading frame together with a Kozak sequence (GCCACC), the human Growth Hormone (hGH) polyadenylation signal and an additional polyadenylation signal. The RMCE vector was transfected into the Taconic Biosciences C57Bl/6 ES cell line equipped with RMCE docking sites in the ROSA26 locus. The ES cell line pre-equipped with F3/FRT - RMCE docking sites was grown on a mitotically inactivated feeder layer comprised of mouse embryonic fibroblasts in ES cell culture medium containing Leukemia inhibitory factor and Fetal Bovine Serum. The cells were co-transfected with the circular exchange vector containing the transgene and the recombinase pCAG-Flpe pA. The transfection was performed via lipofection with a commercially available kit. From day 2 onwards, the medium was replaced daily with medium containing the appropriate selection antibiotics. The recombinant clones were isolated using positive Neomycin resistance selection. On day 7 after transfection, resistant ES cell colonies (ES clones) with a distinct morphology were isolated. The clones were expanded and frozen in liquid nitrogen after extensive molecular validation by Southern Blotting and/or PCR. Quality control of the ES cell line used for transfection was performed at Chrombios GmbH (Germany). Karyotype analysis was undertaken by multicolor fluorescence in situ hybridization with probes for all murine chromosomes (mFISH) to confirm that the cell line meets the quality standard for parental ES cell lines used for targeting experiments. In order to generate chimeras, superovulated BALB/c females were mated with BALB/c males following hormone administration. Blastocysts were isolated from the uterus at dpc 3.5. For microinjection, blastocysts were placed in a drop of DMEM with 15% FCS under mineral oil. A flat tip, piezo actuated microinjection-pipette with an internal diameter of 12 - 15 micrometer was used to inject 10-15 targeted C57BL/6NTac ES cells into each blastocyst. After recovery, 8 injected blastocysts were transferred to each uterine horn of 2.5 days post coitum, pseudopregnant NMRI females. Chimerism was measured in chimeras (G0) by coat color contribution of ES cells to the BALB/c host (black/white). Germline transmission occurred during an IVF expansion using chimeric males and C57BL/6NTac oocyte donors. The colony is maintained by mating wildtype C57BL/6NTac females to heterozygous males and heterozygous females to wildtype C57BL/6NTac males.

Mouse genotyping

Genotyping of mice was performed by the MRC genotyping team at the MRC-PPU, University of Dundee, by PCR using genomic DNA isolated from ear biopsies. For this purpose, Primer 1 (5' CACACACATGGTACACAGATATACATGTAGG 3') Primer 2 (5' ACATCCATGACACGACTCTACTATAGAGAT 3') and Primer 3 (5' CTATCCCGACCGCCTTACTGC 3') were used to distinguish between wildtype and Rab29 knock-out alleles (63°C annealing temp). The VPS35[D620N] knock-in mouse strain required Primer 1 (5' TCATTCTGTGGTTAGTTCAGTTGAG 3'), Primer 2 (5' CCTCTAACAACCAAGAGGAACC 3'), and Primer 3 (5' ATTGCATCGCATTGTCTGAG 3') to distinguish wildtype from D620N knock-in alleles (60°C annealing temp). The LRRK2[R1441C] knock-in mouse strain required Primer 1 (5' CTGCAGGCTACTAGATGGTCAAGGT 3') and Primer 2 (5' CTAGATAGGACCGAGTGTCGCAGAG 3') to identify wildtype and R1441C knock-in alleles (60°C annealing temp). To detect the constitutive KI allele in the transgenic Rab29 overexpression mouse, Primer 1 (5' TTGGGTCCACTCAGTAGATGC 3') and Primer 2 (5' CATGTCTTTAATCTACCTCGATGG 3') as well as internal PCR control Primer 1 (5' GTGGCACGGAACTTCTAGTC 3') and Primer 2 (5' CTTGTCAAGTAGCAGGAAGA 3') were used (58°C annealing temp). To detect the wildtype allele in the transgenic Rab29 overexpression model, Primer 1 (5' CTCTTCCCTCGTGATCTGCAACTCC 3') and Primer 2 (5' CATGTCTTTAATCTACCTCGATGG 3') and internal PCR control Primer 1 (5' GAGACTCTGGCTACTCATCC 3') and Primer 2 (5' CCTTCAGCAAGAGCTGGGGAC 3') were used (58°C annealing temp). All genotyping primers were used at a final concentration of 10 pmol/μl. PCR reactions were set up and run using KOD Hot Start Polymerase standard protocol. PCR bands were visualized on Qiaexcel (Qiagen) using the standard DNA screening kit cartridge.

Preparation of mouse tissue lysates

Mouse tissues were collected and rapidly frozen in liquid nitrogen. Snap frozen tissues were weighed and quickly thawed on ice in a 10-fold volume excess of in ice-cold lysis buffer containing 50 mM Tris/HCl pH 7.4, 1 mM EGTA, 1 mM sodium orthovanadate, 10 mM 2-glycerophosphate, 50 mM NaF, 5 mM sodium pyrophosphate, 270 mM sucrose, supplemented with 1 μg/ml microcystin-LR, 1 mM sodium orthovanadate, complete EDTA-free protease inhibitor cocktail (Roche), and 1% (v/v) Triton X-100. Tissue was homogenized using a POLYTRON homogenizer (KINEMATICA), employing 3 rounds of 10 s homogenization with 10 s intervals on ice. Lysates were centrifuged at 20800 g for 30 min at 4°C and supernatant was collected for subsequent Bradford assay and immunoblot analysis.

Quantitative real time RT-PCR analysis of Rab29 mRNA from mouse tissue

Frozen tissue samples were ground to a fine powder in a vessel submerged in liquid nitrogen using a mallet. ~5 mg tissue was dissolved in lysis buffer provided by RNeasy micro kit (Qiagen), supplemented with 1% (v/v) β-mercaptoethanol. Tissue was homogenized in lysis buffer using IKA VIBRAX VXR basic orbital shaker for 5 min at 4°C at 1000 rpm and total RNA was extracted from tissue lysate following RNeasy micro kit instructions. cDNA was synthesized from total RNA extracts using Bio-Rad iScript cDNA synthesis kit (#170-8891), using a starting template of 150 ng total RNA. The Bio-Rad Sso EvaGreen Supermix (#1725201) was used to set up qPCR reactions in a 384-well plate format according to the manufacturer's instructions, and 20 μl reactions were prepared in duplicate. Real-time

quantitative PCR primers for mouse Rab29 were designed using NCBI Primer Blast and the sequences are as follows: 5'-AGGCCATGAGAGTCCTCGTT-3' (forward) and 5'-GGGCTTGGCTTGGAGATTTGA-3' (reverse). The β-actin internal control primers employed for real-time quantitative PCR analysis are described in [51]: 5'-CACTATCGGCAATGAGCGGTTCC-3' (forward) and 5'-CAGCACTGTGTTGGCATAGAGGTC-3' (reverse). Primers were ordered from Sigma as lyophilized and reconstituted in Milli-Q water to a stock concentration of 100 μM and further diluted to a 10 μM working stock. The PCR efficiency of the aforementioned primers was validated using the relative standard curve method. The qPCR reactions were run using the Bio-Rad CFX384 Real-Time System C1000 Thermal Cycler, and raw data was collected of duplicate reactions from four biological replicates per genotype for three different tissues. The relative quantification of Rab29 and β-actin mRNA was undertaken using the comparative Ct (cycle threshold) method, which employs the formula RQ = $2^{(-\Delta\Delta Ct)}$ [52].

Cell Culture, Treatments, and Lysis

MEFs were cultured in Dulbecco's modified eagle medium (DMEM) supplemented with 10% (v/v) fetal calf serum, 2 mM L-glutamine, 100 U/ml penicillin, 100 μg/ml streptomycin, non-essential amino acids and 1 mM sodium pyruvate. Primary lung fibroblasts were cultured in Dulbecco's modified eagle medium: nutrient mixture F-12 (DMEM/F-12) supplemented with 20% (v/v) fetal calf serum, 2 mM L-glutamine, 100 U/ml penicillin, 100 μg/ml streptomycin, non-essential amino acids and 1 mM sodium pyruvate. All cells were grown at 37°C and 5% CO2 in a humidified atmosphere. Cell lines utilized for this study were tested regularly for mycoplasma contamination and confirmed as negative prior to experimental analysis. Cells were lysed in ice-cold lysis buffer containing 50 mM Tris/HCl pH 7.4, 1 mM EGTA, 1 mM sodium orthovanadate, 10 mM 2-glycerophosphate, 50 mM NaF, 5 mM sodium pyrophosphate, 270 mM sucrose, supplemented with 1 μg/ml microcystin-LR, 1 mM sodium orthovanadate, complete EDTA-free protease inhibitor cocktail (Roche), and 1% (v/v) Triton X-100. Lysates were clarified by centrifugation for 15 min at 15,000 g at 4°C. Protein concentrations of cell lysates were determined using the Bradford assay.

Generation of mouse embryonic fibroblasts (MEFs)

Wildtype, heterozygous, and homozygous Rab29 knock-out or transgenic Rab29 overexpressing MEFs were isolated from littermate-matched mouse embryos at day E12.5, as described in a previous study [53]. The resulting embryo genotypes were produced following crosses between Rab29 knock-out/wildtype (heterozygous) mice or between transgenic Rab29/wildtype (heterozygous) mice. Rab29 knock-out and LRRK2[R1441C] mice were bred to create doubly modified Rab29 knock-out/LRRK2[R1441C], and Rab29-knock-out and VPS35[D620N] mice were bred to create doubly modified Rab29 knock-out/VPS35[D620N] mice. To generate MEFs for these mouse models, the following crosses between homozygous mice of the following genotypes were set up: Rab29 wildtype/LRRK2 or VPS35 wildtype, Rab29 knock-out/LRRK2 or VPS35 wildtype, Rab29 wildtype/LRRK2[R1441C] or VPS35[D620N], and Rab29 knock-out/LRRK2[R1441C] or VPS35[D620N]. The resulting embryos from each litter were of the same genotype and MEFs were isolated at day E12.5. Genotypes of all aforementioned mouse models were verified via allelic sequencing and immunoblot. Primary MEFs between passage 2 and 8 were used for all experimental analyses.

siRNA-mediated knockdown of target proteins in MEFs

For siRNA knockdown of proteins of interest, ON-TARGETplus Mouse LRRK2 siRNA-SMARTpool (#L-049666-00-0005), ON-TARGETplus Mouse Rab32 siRNA-SMARTpool (#L-063539-01-0005) and ON-TARGETplus non-targeting pool (#D-001810-10-05) were purchased from Dharmacon. MEF cells were seeded in a 6-well format at 400,000 cells/well for transfection the following day. Cells were transfected using Lipofectamine RNAiMAX according to the manufacturer's protocol. Briefly, 50 pmol siRNA was diluted in 150 µl opti-MEM and combined with 10 µl Lipofectamine RNAiMAX in 150 µl opti-MEM per well. The two mixes were incubated together at room temperature for 5 min and 250 µL was added dropwise to cells, which were harvested 72 hours after transfection.

MLi-2 inhibitor washout in MEFs

Primary MEFs of the indicated genotypes in Figure 7 were seeded in a 6-well format for treatment the following day. At ~50-60% confluence, MEFs were treated with vehicle (DMSO) or 100 nM MLi-2 for 48 hours. To remove the MLi-2 inhibitor, cells were washed three times with warm, complete media. 15-20 min following the initial washes, cells were washed an additional two times with complete media. Cells were harvested with complete lysis buffer 30-360 min following the initial washes.

Generation of primary lung fibroblasts

Primary lung fibroblasts were derived from adult mice as previously described [54]. Briefly, lung tissue was harvested from mice and transferred to a sterile tissue culture dish, washed twice with PBS and minced with a scalpel. Tissue fragments were transferred to a 75cm^2 cell culture flask with suitable aeration, and immersed in 10ml DMEM/F12 supplemented with 2 mM L-glutamine, 100 U/ml penicillin, 100 µg/ml streptomycin, and 0.14 Wunsch units/ml collagenase (Liberase, Sigma-Aldrich 05401119001). The tissue fragments were digested with collagenase in a shaking incubator at 37°C and 5% CO2 for one hour. 20ml of DMEM/F12 supplemented with 20% (v/v) fetal calf serum, 2mM L-glutamine, 100 U/ml penicillin, and 100 µg/ml streptomycin was added, and the cell/tissue suspension was centrifuged at room temperature at 525 g for 5 min. The pellet was gently resuspended in fresh complete media and plated in a collagen-coated cell culture flask. To coat the cell culture flasks, Gibco Collagen I, rat tail (A10483-01) was diluted to a final concentration of 50 µg/ml in sterile-filtered 20 mM acetic acid. Tissue-culture flasks were coated with diluted collagen according to the manufacturer's protocol. Fibroblasts required ~5 days to emerge from tissue fragments and regular media changes. Approximately 1.5 weeks following isolation, lung fibroblasts were passaged once, then seeded in 6-well plates for experimental analysis.

Results

Expression of Rab29 in mouse tissues and cells

We raised two novel Rab29 monoclonal antibodies termed MJF-30-Clone-124 and MJF-30-Clone-104 that detect endogenous Rab29 in wildtype but not in Rab29 knock-out human A549 cells (Fig 1A). MJF-30-Clone-124 detected both mouse and human Rab29 whilst MJF-30-Clone-104 was human specific (Fig 1A). Immunoblotting of 6 mouse tissues (brain, spleen, lung, kidney, large intestine and spinal cord) and 3 primary mouse cell lines (mouse embryonic fibroblasts (MEFs), lung fibroblasts and bone marrow derived macrophages) that all express endogenous LRRK2, revealed that Rab29 is expressed ubiquitously but levels vary significantly between tissues and cells (Fig 1B). Highest expression is observed in macrophages and spleen, with low expression seen in brain and spinal cord, with intermediate expression in other tissues and cells. LRRK2 was proteolyzed in at least two bands in many extracts but the expression of the two major upper bands was also lower in brain and spinal cord, and significantly higher levels in other tissues and cells.

Rab29 knock-out does not impact basal LRRK2-mediated phosphorylation of Rab10 in mouse tissues and MEFs

To investigate the role that endogenous Rab29 plays in regulating LRRK2 pathway activity, we obtained Rab29 knock-out mice made available through the Wellcome Trust Sanger Institute, Infrafrontier EMMA mouse repository and the Michael J. Fox Foundation (see Methods). These mice have also been deployed in other studies mentioned in the Introduction [42,43,45]. As a readout for LRRK2 pathway activity we measured phosphorylation of Rab10 at Thr73 [7], employing a well-characterized phospho-specific antibody [50]. Consistent with previous reports [43], the Rab29 knock-out mice were viable and displayed no overt phenotypes. We analyzed wildtype, heterozygous and Rab29 knock-out MEFs (Fig 2A) as well as wildtype and Rab29 knock-out lung (Fig 2B), spleen (Fig 2C), kidney (Fig 2D) and various brain sections (Fig S1) derived from littermate 6-month-old mice treated ± MLi-2 LRRK2 inhibitor (30 mg/kg, 2 h). Results from numerous independent experiments demonstrated that there was no significant difference in levels of LRRK2-phosphorylated Rab10 quantitated as ratio with total Rab10, in wildtype or Rab29 knock-out MEFs, lung, spleen or kidney. Rab29 knock-out also had no impact on LRRK2 expression or phosphorylation of LRRK2 at Ser935 (Fig 2, S1). As expected, MLi-2 treatment markedly reduced Rab10 phosphorylation levels in both wildtype and Rab29 knock-out mice that was accompanied by a decrease in LRRK2 Ser935 phosphorylation. We found that although MLi-2 administration reduced Ser935 phosphorylation in brain, the low basal levels of pRab10 observed were not further decreased (Fig S1), which is consistent with previous findings [50,55].

Generation and characterization of Rab29 overexpressing transgenic mice

As the human genetic data point toward variants within the PARK16 locus enhancing expression of Rab29 [15,37,38], we generated a transgenic mouse strain in which Rab29 is constitutively overexpressed in all tissues. The mouse Rab29 cDNA with no epitope tags was knocked-into the ROSA26 locus, which is frequently employed to constitutively express proteins in mouse tissues [56] (Fig 3A). The heterozygous and homozygous Rab29 transgenic mice displayed no overt phenotype at 6 months of age which were the oldest animals studied. Rab29 protein levels in brain, spleen, lung, kidney, large intestine and spinal cord derived from wildtype and homozygous transgenic Rab29 mice were analyzed at 3.5 and 6

months of age. This revealed that the highest overexpression of Rab29 was observed in brain (7-9-fold), kidney (5-7-fold) and large intestine (23-25-fold), with lower levels of overexpression observed in lung (<1.5-fold), spleen (<2-fold) and spinal cord (4-fold) (Fig 3B). There was no marked difference in the relative levels of Rab29 expression between 3.5 and 6-month-old mice (Fig 3B). We also analyzed Rab29 mRNA levels in wildtype, heterozygous and homozygous brain, lung and kidney from 3.5-month-old mice (Fig 3C). Consistent with protein levels, brain displayed highest levels of increase in Rab29 mRNA levels, namely 2-fold in heterozygous and ~4-fold in homozygous Rab29 transgenic mice (Fig 3C). In transgenic homozygous kidney and lung, Rab29 mRNA levels were increased under 3 and 2-fold, respectively (Fig 3C).

Transgenic overexpression of Rab29 does not impact basal LRRK2-mediated phosphorylation of Rab10 in mouse tissues and cells

We examined LRRK2-mediated Rab10 phosphorylation in wildtype and homozygous transgenic Rab29 mouse brain (Fig 4A), large intestine (Fig 4B), kidney (Fig 4C), lung (Fig 4D), spleen (Fig 4E) and spinal cord (Fig 4F) from 6-month-old mice treated for two hours ± MLi-2 LRRK2 inhibitor (30 mg/kg). No significant increases in LRRK2-mediated phosphorylation of Rab10 were observed in any of the tissues. Levels of LRRK2 or phosphorylation at Ser935 were also not impacted by Rab29 overexpression. Similar results were also observed in 3.5-month-old animals (Fig S2). We also studied MEFs and lung fibroblasts derived from wildtype and homozygous Rab29 transgenic mice in which Rab29 levels were increased ~4-fold in both cell types, and here again observed no significant impact on LRRK2-mediated Rab10 phosphorylation (Fig S3). We also immunoblotted for Rab12 pSer105 in MEFs and observed no change in phosphorylation following Rab29 overexpression. As expected, MLi-2 reduced Rab12 phosphorylation in this experiment (Fig S3).

Knock-out of Rab29 does not reduce elevated Rab10 phosphorylation in LRRK2[R1441C] knock-in mice

To study whether endogenous Rab29 was necessary for the previously reported elevated Rab10 phosphorylation observed in LRRK2[R1441C] knock-in MEFs and mouse tissues [26,50], we generated LRRK2[R1441C] knock-in MEFs as well as 6-month-old LRRK2[R1441C] ± Rab29 knock-out mice. As a control to demonstrate that the LRRK2[R1441C] pathogenic mutation enhanced Rab10 phosphorylation, we also generated matched LRRK2 wildtype ± Rab29 knock-out for comparison. In MEFs, as reported previously [50], LRRK2[R1441C] knock-in mutation enhanced Rab10 phosphorylation around 3-fold (Fig 5A). Knock-out of Rab29 had no impact on Rab10 phosphorylation (Fig 5A). As reported previously [57], the R1441C mutation reduced Ser935 phosphorylation, which was also not impacted by Rab29 knock-out (Fig 5A). In mouse lung (Fig 5B), kidney (Fig 5C), spleen (Fig 5D), large intestine (Fig S4A), brain (Fig S4B) and spinal cord (Fig S4C), we also observed that knock-out of Rab29 in LRRK2[R1441C] knock-in mice had no significant impact on Rab10 phosphorylation. The LRRK2[R1441C] mutation enhanced Rab10 phosphorylation between 1.5 to 2-fold in lung (Fig 5B), kidney (Fig 5C), spleen (Fig 5D), and large intestine (Fig S4A). No significant increase in Rab10 phosphorylation was observed in the brain (Fig S4B) and spinal cord (Fig S4C) of LRRK2[R1441C] knock-in mice. However, moderate sensitivity to MLi-2 was observed in the LRRK2[R1441C] knock-in mice not observed in wildtype animals (Fig S4B).

Knock-out of Rab29 does not reduce elevated Rab10 phosphorylation in VPS35[D620N] knock-in mice

To investigate whether endogenous Rab29 was necessary for the elevated Rab10 phosphorylation observed in VPS35[D620N] MEFs and mouse tissues [21], we generated VPS35[D620N] knock-in MEFs and 6-month-old VPS35[D620N] ± Rab29 knock-out mice. As a control, we also generated matched VPS35 wildtype ± Rab29 knock-out animals. As reported previously [21], VPS35[D620N] knock-in mutation enhanced Rab10 phosphorylation to a greater extent than is observed with the LRRK2[R1441C] pathogenic mutation (compare Fig 5 with Fig 6). Knock-out of Rab29 had no significant impact on the elevated Rab10 phosphorylation in the VPS35[D620N] knock-in MEFs (Fig 6A) or in mouse lung (Fig 6B), kidney (Fig 6C), spleen (Fig 6D), large intestine (Fig S5A), and spinal cord (Fig S5C). In brain derived from VPS35[D620N] animals, a moderate 1.5-fold increase in Rab10 phosphorylation was observed, which decreased with MLi-2 administration, but was also not significantly impacted by Rab29 knock-out (Fig S5B). Consistent with previous results [21], the phosphorylation of Ser935 was not impacted by the VPS35[D620N] mutation. Knock-out of Rab29 had no impact on Ser935 phosphorylation in these MEFs and mouse tissues (Fig 6).

Rate of recovery of Rab10 phosphorylation after washout of MLi-2 LRRK2 inhibitor is not impacted by Rab29 knock-out

We next investigated whether endogenous Rab29 affected the rate at which Rab10 was re-phosphorylated following washout of MLi-2 in MEFs. We treated wildtype (Fig 7A), LRRK2[R1441C] (Fig 7B) or VPS35[D620N] (Fig 7C) ± Rab29 knock-out MEFs with MLi-2 to reduce pRab10 to undetectable levels (100 nM, 48 hours). MLi-2 was removed by several changes of medium over a 15 min period, and phosphorylation of Rab10 quantified at time points up to 6 hours. Under these conditions we observed that the rate of recovery in the 3 cell lines was not affected by Rab29 knock-out. For the wildtype and VPS35[D620N] MEFs we observed 60-70% recovery of Rab10 phosphorylation within 6 hours. However, in the LRRK2[R1441C] MEFs, recovery of pRab10 was only ~30% after 6 hours, and it is possible that the higher affinity of MLi-2 for this pathogenic mutant might account for this.

Evidence that Rab32 is not compensating for loss of Rab29 in regulating LRRK2

Finally, we explored whether Rab32, which is closely related to Rab29 and reported to interact with LRRK2 [40,58], could contribute to regulation of LRRK2 activity in Rab29 knock-out MEFs. siRNA knockdown reduced Rab32 expression by 70-80%, but this had no impact on Rab10 phosphorylation in Rab29 knock-out wildtype LRRK2 or LRRK2[R1441C] knock-in cells (Fig 8). Knockdown of LRRK2 in parallel experiments, as expected, markedly reduced Rab10 phosphorylation (Fig 8). By immunoblotting analysis of wildtype and Rab29 knock-out MEFs, we were unable to detect Rab38, which is also related to Rab29 and Rab32. This is consistent with previous high-resolution proteomic analysis of MEFs in which Rab38 was not detected [7].

Discussion

As outlined in the introduction, biochemical, cellular and genetic evidence undertaken by different researchers supports the view that transient overexpression of Rab29 recruits the bulk of cellular LRRK2 to the Golgi surface, leading to its activation. In overexpression studies the LRRK2[R1441C/G] mutants are more readily activated by Rab29, which could explain why this mutation elevates LRRK2 activity. However, our results suggest that knock-out of endogenous Rab29 has no significant impact on endogenous LRRK2 activity, that we assessed by monitoring pRab10 levels in six different mouse tissues as well as MEFs and lung derived fibroblasts. Moreover, we also found that knock-out of Rab29 does not impact elevated Rab10 phosphorylation observed in the LRRK2[R1441C] knock-in MEFs or mouse tissues. This would suggest that endogenous Rab29 is not sufficient to explain the elevated activity of the LRRK2[R1441C] pathogenic mutant. We also found that Rab29 knock-out had no effect on the elevated LRRK2-mediated Rab10 phosphorylation observed in VPS35[D620N] knock-in MEFs and mouse tissues. To our knowledge, there is no evidence implicating Rab29 in mediating the effects of the VPS35[D620N] mutation.

It is possible that other Rab proteins, or even other regulators that have not yet been characterized, could also interact with and activate LRRK2 in a similar manner to Rab29, by recruiting LRRK2 to a variety of cellular membranes. In the absence of Rab29 overexpression, LRRK2 is widely distributed in cells with ~90% cytosolic localization, and ~10% localized on a variety of cellular membranes [14,59–61]. A small fraction of LRRK2 appears to be localized in the Golgi region without Rab29 overexpression [14–17,62], which may explain why Rab29 knock-out does not have a noticeable impact on Rab10 protein phosphorylation when measured in a whole cell or tissue extract. In future work, it will be important to develop assays in which the pool of endogenous LRRK2 that resides at the Golgi could be specifically assessed. Since LRRK2 is likely in equilibrium between membranes and the cytosol [29], such interactions may be transient and more challenging to capture quantitatively. Indeed, by elevating the local concentration of Rab29 on the Golgi by exogenous expression, this pool was more readily detected. It will be critical to establish whether the activity and localization of the endogenous pool of Golgi-resident LRRK2 is dependent upon Rab29. It will also be necessary to study further whether endogenous LRRK2 located on other specific membrane compartments relies on other Rab proteins or regulators for this localization, and whether this contributes to the total cellular LRRK2 activity measured in cell extracts. It would also be important to define more precisely the residues in LRRK2 that bind Rab29 and investigate how subtle mutations that prevent Rab29 binding, impact cellular LRRK2 activity. Whether other Rab proteins bind to the same or different sites in LRRK2 should also be investigated.

The ability of exogenous Rab29 to recruit LRRK2 to the Golgi (or other compartments to which it is targeted) confirms the ability of Rab29 to bind LRRK2 in cells. Yet our knock-in and knock-out models failed to reveal clues to the functional significance of this interaction. Rab29 is a relatively poorly abundant Rab and may play a specific role in macrophages and dendritic cells where it is most abundant. Indeed, LRRK2 activation triggered by Rab29 could occur in a specific cell type or tissue, or following a physiological stimulus, stress or infection that we have not investigated. Our data do not rule out the possibility that Rab29 knock-out is compensated by another cellular protein(s) other than Rab32. However, our findings with transgenic mice that overexpress Rab29 from 1.5 to 25-fold, without enhancing LRRK2-

mediated Rab10 phosphorylation, reveal that increasing Rab29 expression is not sufficient to stimulate the activity of endogenous LRRK2.

We have shown previously that Rab3, Rab8A, Rab10 Rab12, Rab35 and Rab43 are the main substrates of LRRK2 [7,26,63] and here have monitored changes in phosphorylation of Rab10 and Rab12. We therefore cannot exclude the possibility that Rab29 preferentially activates phosphorylation of the Rab proteins we have not assayed, but we consider this unlikely because this set of Rab proteins appear to be coordinately phosphorylated in all cultured cell experiments that we have carried out to date [26,50,64]. It has also been suggested that screens could be undertaken to identify potentially therapeutic compounds that block Rab29 binding to LRRK2, however our data suggest that such agents may not be effective at reducing basal LRRK2 activity, unless these chemicals also block LRRK2 binding to other regulators that take it to cellular membranes. Finally, we propose that the new Rab29 monoclonal antibodies we have developed could be exploited to better understand how Parkinson's mutations within the PARK16 locus impact Rab29 protein expression.

Acknowledgements
We thank Suzanne Pfeffer (Stanford) and Shalini Padmanabhan (The Michael J. Fox Foundation for Parkinson's Research) for helpful discussions, Gail Gilmour and Shauna Channon for mouse genotyping, and the excellent technical support of the MRC-Protein Phosphorylation and Ubiquitylation Unit (PPU), including the MRC-PPU tissue culture team (coordinated by Edwin Allen) and MRC PPU Reagents and Services antibody teams (coordinated by Hilary McLauchlan and James Hastie).

Funding
A.F.K. is generously supported by a Parkinson's UK Studentship H-1701. This work was supported by The Michael J. Fox Foundation for Parkinson's Research [grant number 17298 (D.R.A.)] and [grant number 6986 (D.R.A.)], the Medical Research Council [grant number MC_UU_12016/2 (D.R.A.)] and the pharmaceutical companies supporting the Division of Signal Transduction Therapy Unit (Boehringer-Ingelheim, GlaxoSmithKline, Merck KGaA -to D.R.A.).

Author Contributions
A.F.K designed, executed all experiments in this study apart from Figure 1A, analyzed and interpreted data and wrote the manuscript with D.R.A. P.L. designed and executed experiments that led to the development and characterization of the Rab29 MJF-30 Clone-104 & Clone-124 antibodies as well as undertaking work shown in Figure 1A. N.K.P. oversaw and coordinated the generation of the Rab29 transgenic mice as well as the Rab29 MJF-30 antibodies. D.R.A. helped with experimental design, analysis and interpretation of data and wrote the paper with A.F.K.

References

1 Zimprich, A., Biskup, S., Leitner, P., Lichtner, P., Farrer, M., Lincoln, S., Kachergus, J., Hulihan, M., Uitti, R. J., Calne, D. B., et al. (2004) Mutations in LRRK2 cause autosomal-dominant parkinsonism with pleomorphic pathology. Neuron **44**, 601–607.

2 Paisán-Ruíz, C., Jain, S., Evans, E. W., Gilks, W. P., Simón, J., Van Der Brug, M., De Munain, A. L., Aparicio, S., Gil, A. M., Khan, N., et al. (2004) Cloning of the gene containing mutations that cause PARK8-linked Parkinson's disease. Neuron **44**, 595–600.

3 Taylor, M. and Alessi, D. R. (2020) Advances in elucidating the function of leucine-rich repeat protein kinase-2 in normal cells and Parkinson's disease. Curr. Opin. Cell Biol., Elsevier Ltd **63**, 102–113.

4 Domingo, A. and Klein, C. (2018) Genetics of Parkinson disease. Handb. Clin. Neurol. 1st ed., Elsevier B.V.

5 Price, A., Manzoni, C., Cookson, M. R. and Lewis, P. A. (2018, July 1) The LRRK2 signalling system. Cell Tissue Res., Springer Verlag.

6 Jaleel, M., Nichols, R. J., Deak, M., Campbell, D. G., Gillardon, F., Knebel, A. and Alessi, D. R. (2007) LRRK2 phosphorylates moesin at threonine-558: Characterization of how Parkinson's disease mutants affect kinase activity. Biochem. J. **405**, 307–317.

7 Steger, M., Tonelli, F., Ito, G., Davies, P., Trost, M., Vetter, M., Wachter, S., Lorentzen, E., Duddy, G., Wilson, S., et al. (2016) Phosphoproteomics reveals that Parkinson's disease kinase LRRK2 regulates a subset of Rab GTPases. Elife **5**.

8 West, A. B., Moore, D. J., Biskup, S., Bugayenko, A., Smith, W. W., Ross, C. A., Dawson, V. L. and Dawson, T. M. (2005) Parkinson's disease-associated mutations in leucine-rich repeat kinase 2 augment kinase activity. Proc. Natl. Acad. Sci. U. S. A. **102**, 16842–16847.

9 Ito, G., Katsemonova, K., Tonelli, F., Lis, P., Baptista, M. A. S., Shpiro, N., Duddy, G., Wilson, S., Ho, P. W. L., Ho, S. L., et al. (2016) Phos-Tag analysis of Rab10 phosphorylation by LRRK2: A powerful assay for assessing kinase function and inhibitors. Biochem. J., Portland Press Ltd **473**, 2671–2685.

10 Sheng, Z., Zhang, S., Bustos, D., Kleinheinz, T., Le Pichon, C. E., Dominguez, S. L., Solanoy, H. O., Drummond, J., Zhang, X., Ding, X., et al. (2012) Ser1292 autophosphorylation is an indicator of LRRK2 kinase activity and contributes to the cellular effects of PD mutations. Sci. Transl. Med. **4**.

11 Lewis, P. A., Greggio, E., Beilina, A., Jain, S., Baker, A. and Cookson, M. R. (2007) The R1441C mutation of LRRK2 disrupts GTP hydrolysis. Biochem. Biophys. Res. Commun. **357**, 668–671.

12 Li, X., Tan, Y. C., Poulose, S., Olanow, C. W., Huang, X. Y. and Yue, Z. (2007) Leucine-rich repeat kinase 2 (LRRK2)/PARK8 possesses GTPase activity that is altered in familial Parkinson's disease R1441C/G mutants. J. Neurochem. **103**, 238–247.

13 Liao, J., Wu, C. X., Burlak, C., Zhang, S., Sahm, H., Wang, M., Zhang, Z. Y., Vogel, K. W., Federici, M., Riddle, S. M., et al. (2014) Parkinson disease-associated mutation R1441H in LRRK2 prolongs the "active state" of its GTPase domain. Proc. Natl. Acad. Sci. U. S. A., National Academy of Sciences **111**, 4055–4060.

14 Purlyte, E., Dhekne, H. S., Sarhan, A. R., Gomez, R., Lis, P., Wightman, M., Martinez, T. N., Tonelli, F., Pfeffer, S. R. and Alessi, D. R. (2018) Rab29 activation of the Parkinson's disease-associated LRRK2 kinase. EMBO J **37**, 1–18.

15 Beilina, A., Rudenko, I. N., Kaganovich, A., Civiero, L., Chau, H., Kalia, S. K., Kalia, L. V, Lobbestael, E., Chia, R., Ndukwe, K., et al. (2014) Unbiased screen for interactors of leucine-

rich repeat kinase 2 supports a common pathway for sporadic and familial Parkinson disease. Proc Natl Acad Sci U S A **111**, 2626–2631.

16 Liu, Z., Bryant, N., Kumaran, R., Beilina, A., Abeliovich, A., Cookson, M. R. and West, A. B. (2018) LRRK2 phosphorylates membrane-bound Rabs and is activated by GTP-bound Rab7L1 to promote recruitment to the trans-Golgi network. Hum Mol Genet **27**, 385–395.

17 Fujimoto, T., Kuwahara, T., Eguchi, T., Sakurai, M., Komori, T. and Iwatsubo, T. (2018) Parkinson's disease-associated mutant LRRK2 phosphorylates Rab7L1 and modifies trans-Golgi morphology. Biochem Biophys Res Commun **495**, 1708–1715.

18 Watanabe, R., Buschauer, R., Böhning, J., Audagnotto, M., Lasker, K., Wen Lu, T., Boassa, D., Taylor, S. S. and Villa, E. (2020) The In situ Structure of Parkinson's Disease-Linked LRRK2. Biophys. J. **118**, 486a.

19 Deniston, C. K., Salogiannis, J., Mathea, S., Snead, D. M., Lahiri, I., Donosa, O., Watanabe, R., Böhning, J., Shiau, A. K., Knapp, S., et al. (2020) Parkinson ' s Disease-linked LRRK2 structure and model for microtubule interaction. bioRxiv **2**, 1–11.

20 Schmidt, S. H., Knape, M. J., Boassa, D., Mumdey, N., Kornev, A. P., Ellisman, M. H., Taylor, S. S. and Herberg, F. W. (2019) The dynamic switch mechanism that leads to activation of LRRK2 is embedded in the DFGψ motif in the kinase domain. Proc. Natl. Acad. Sci. U. S. A., National Academy of Sciences **116**, 14979–14988.

21 Mir, R., Tonelli, F., Lis, P., Macartney, T., Polinski, N. K., Martinez, T. N., Chou, M. Y., Howden, A. J. M., Konig, T., Hotzy, C., et al. (2018) The Parkinson's disease VPS35[D620N] mutation enhances LRRK2-mediated Rab protein phosphorylation in mouse and human. Biochem J **475**, 1861–1883.

22 Doggett, E. A., Zhao, J., Mork, C. N., Hu, D. and Nichols, R. J. (2012) Phosphorylation of LRRK2 serines 955 and 973 is disrupted by Parkinson's disease mutations and LRRK2 pharmacological inhibition. J. Neurochem. **120**, 37–45.

23 Dzamko, N., Deak, M., Hentati, F., Reith, A. D., Prescott, A. R., Alessi, D. R. and Nichols, R. J. (2010) Inhibition of LRRK2 kinase activity leads to dephosphorylation of Ser 910/Ser935, disruption of 14-3-3 binding and altered cytoplasmic localization. Biochem. J. **430**, 405–413.

24 Alessi, D. R. and Sammler, E. (2018, April 6) LRRK2 kinase in Parkinson's disease. Science (80-.)., American Association for the Advancement of Science.

25 Tolosa, E., Vila, M., Klein, C. and Rascol, O. (2020) LRRK2 in Parkinson disease: challenges of clinical trials. Nat. Rev. Neurol., Springer US **16**, 97–107.

26 Steger, M., Diez, F., Dhekne, H. S., Lis, P., Nirujogi, R. S., Karayel, O., Tonelli, F., Martinez, T. N., Lorentzen, E., Pfeffer, S. R., et al. (2017) Systematic proteomic analysis of LRRK2-mediated Rab GTPase phosphorylation establishes a connection to ciliogenesis. Elife **6**.

27 Pfeffer, S. R. (2017, March 15) Rab GTPases: Master regulators that establish the secretory and endocytic pathways. Mol. Biol. Cell, American Society for Cell Biology.

28 Jeong, G. R., Jang, E. H., Bae, J. R., Jun, S., Kang, H. C., Park, C. H., Shin, J. H., Yamamoto, Y., Tanaka-Yamamoto, K., Dawson, V. L., et al. (2018) Dysregulated phosphorylation of Rab GTPases by LRRK2 induces neurodegeneration. Mol. Neurodegener., BioMed Central Ltd. **13**, 8.

29 Gomez, R. C., Wawro, P., Lis, P., Alessi, D. R. and Pfeffer, S. R. (2019) Membrane association but not identity is required for LRRK2 activation and phosphorylation of Rab GTPases. J. Cell Biol., NLM (Medline) **218**, 4157–4170.

30 Waschbüsch, D., Purlyte, E., Pal, P., McGrath, E., Alessi, D. R. and Khan, A. R. (2020) Structural

Basis for Rab8a Recruitment of RILPL2 via LRRK2 Phosphorylation of Switch 2. Structure, Cell Press **28**, 406-417.e6.

31 Dhekne, H. S., Yanatori, I., Gomez, R. C., Tonelli, F., Diez, F., Schüle, B., Steger, M., Alessi, D. R. and Pfeffer, S. R. (2018) A pathway for parkinson's disease LRRK2 kinase to block primary cilia and sonic hedgehog signaling in the brain. Elife, eLife Sciences Publications Ltd **7**.

32 Sobu, Y., Wawro, P. S., Dhekne, H. S. and Pfeffer, S. R. (2020) Pathogenic LRRK2 regulates ciliation probability upstream of Tau Tubulin kinase 2. bioRxiv, Cold Spring Harbor Laboratory 2020.04.07.029983.

33 Lill, C. M., Roehr, J. T., McQueen, M. B., Kavvoura, F. K., Bagade, S., Schjeide, B. M., Schjeide, L. M., Meissner, E., Zauft, U., Allen, N. C., et al. (2012) Comprehensive research synopsis and systematic meta-analyses in Parkinson's disease genetics: The PDGene database. PLoS Genet **8**, e1002548.

34 Tucci, A., Nalls, M. A., Houlden, H., Revesz, T., Singleton, A. B., Wood, N. W., Hardy, J. and Paisan-Ruiz, C. (2010) Genetic variability at the PARK16 locus. Eur J Hum Genet **18**, 1356–1359.

35 Simón-Sánchez, J., Schulte, C., Bras, J. M., Sharma, M., Gibbs, J. R., Berg, D., Paisan-Ruiz, C., Lichtner, P., Scholz, S. W., Hernandez, D. G., et al. (2009) Genome-wide association study reveals genetic risk underlying Parkinson's disease. Nat. Genet., Nature Publishing Group **41**, 1308–1312.

36 Satake, W., Nakabayashi, Y., Mizuta, I., Hirota, Y., Ito, C., Kubo, M., Kawaguchi, T., Tsunoda, T., Watanabe, M., Takeda, A., et al. (2009) Genome-wide association study identifies common variants at four loci as genetic risk factors for Parkinson's disease. Nat. Genet., Nature Publishing Group **41**, 1303–1307.

37 Nalls, M. A., Pankratz, N., Lill, C. M., Do, C. B., Hernandez, D. G., Saad, M., DeStefano, A. L., Kara, E., Bras, J., Sharma, M., et al. (2014) Large-scale meta-analysis of genome-wide association data identifies six new risk loci for Parkinson's disease. Nat Genet **46**, 989–993.

38 MacLeod, D. A., Rhinn, H., Kuwahara, T., Zolin, A., Di Paolo, G., MacCabe, B. D., Marder, K. S., Honig, L. S., Clark, L. N., Small, S. A., et al. (2013) RAB7L1 Interacts with LRRK2 to Modify Intraneuronal Protein Sorting and Parkinson's Disease Risk. Neuron, Elsevier **77**, 425–439.

39 Pihlstrøm, L., Rengmark, A., Bjørnarå, K. A., Dizdar, N., Fardell, C., Forsgren, L., Holmberg, B., Larsen, J. P., Linder, J., Nissbrandt, H., et al. (2015) Fine mapping and resequencing of the PARK16 locus in Parkinson's disease. J. Hum. Genet. **60**, 357–362.

40 McGrath, E., Waschbüsch, D., Baker, B. M. and Khan, A. R. (2019) LRRK2 binds to the Rab32 subfamily in a GTP-dependent manner via its armadillo domain. Small GTPases, Taylor & Francis **00**, 1–14.

41 Dodson, M. W., Zhang, T., Jiang, C., Chen, S. and Guo, M. (2012) Roles of the Drosophila LRRK2 homolog in Rab7-dependent lysosomal positioning. Hum. Mol. Genet. **21**, 1350–1363.

42 Kuwahara, T., Inoue, K., D'Agati, V. D., Fujimoto, T., Eguchi, T., Saha, S., Wolozin, B., Iwatsubo, T. and Abeliovich, A. (2016) LRRK2 and RAB7L1 coordinately regulate axonal morphology and lysosome integrity in diverse cellular contexts. Sci Rep **6**, 29945.

43 Mazza, M. C., Nguyen, V., Beilina, A., Ding, J. and Cookson, M. R. (2020) Combined knockout of Lrrk2 and Rab29 does not result in behavioral abnormalities in vivo. bioRxiv, Cold Spring Harbor Laboratory 2020.05.13.093708.

44 Wang, S., Ma, Z., Xu, X., Wang, Z., Sun, L., Zhou, Y., Lin, X., Hong, W. and Wang, T. (2014) A role of Rab29 in the integrity of the trans-Golgi network and retrograde trafficking of

mannose-6-phosphate receptor. PLoS One **9**, e96242.

45 Beilina, A., Bonet-Ponce, L., Kumaran, R., Kordich, J. J., Ishida, M., Mamais, A., Kaganovich, A., Saez-Atienzar, S., Gershlick, D. C., Roosen, D. A., et al. (2020) The Parkinson's Disease Protein LRRK2 Interacts with the GARP Complex to Promote Retrograde Transport to the trans-Golgi Network. Cell Rep. **31**.

46 Spanò, S., Liu, X. and Galán, J. E. (2011) Proteolytic targeting of Rab29 by an effector protein distinguishes the intracellular compartments of human-adapted and broad-host Salmonella. Proc. Natl. Acad. Sci. U. S. A., National Academy of Sciences **108**, 18418–18423.

47 Wasmeier, C., Romao, M., Plowright, L., Bennett, D. C., Raposo, G. and Seabra, M. C. (2006) Rab38 and Rab32 control post-Golgi trafficking of melanogenic enzymes. J Cell Biol **175**, 271–281.

48 Fell, M. J., Mirescu, C., Basu, K., Cheewatrakoolpong, B., DeMong, D. E., Ellis, J. M., Hyde, L. A., Lin, Y., Markgraf, C. G., Mei, H., et al. (2015) MLi-2, a potent, selective, and centrally active compound for exploring the therapeutic potential and safety of LRRK2 kinase inhibition. J. Pharmacol. Exp. Ther. **355**, 397–409.

49 Spieker-Polet, H., Sethupathi, P., Yam, P. C. and Knight, K. L. (1995) Rabbit monoclonal antibodies: Generating a fusion partner to produce rabbit-rabbit hybridomas. Proc. Natl. Acad. Sci. U. S. A. **92**, 9348–9352.

50 Lis, P., Burel, S., Steger, M., Mann, M., Brown, F., Diez, F., Tonelli, F., Holton, J. L., Ho, P. W., Ho, S. L., et al. (2018) Development of phospho-specific Rab protein antibodies to monitor in vivo activity of the LRRK2 Parkinson's disease kinase. Biochem. J. **475**, 1–22.

51 Liang, Y., Lin, S., Zou, L., Zhou, H., Zhang, J., Su, B. and Wan, Y. (2012) Expression profiling of Rab GTPases reveals the involvement of Rab20 and Rab32 in acute brain inflammation in mice. Neurosci Lett **527**, 110–114.

52 Livak, K. J. and Schmittgen, T. D. (2001) Analysis of relative gene expression data using real-time quantitative PCR and the 2-ΔΔCT method. Methods **25**, 402–408.

53 Wiggin, G. R., Soloaga, A., Foster, J. M., Murray-Tait, V., Cohen, P. and Arthur, J. S. C. (2002) MSK1 and MSK2 Are Required for the Mitogen- and Stress-Induced Phosphorylation of CREB and ATF1 in Fibroblasts. Mol. Cell. Biol. **22**, 2871–2881.

54 Tian, X., Azpurua, J., Hine, C., Vaidya, A., Myakishev-Rempel, M., Ablaeva, J., Mao, Z., Nevo, E., Gorbunova, V. and Seluanov, A. (2013) High-molecular-mass hyaluronan mediates the cancer resistance of the naked mole rat. Nature **499**, 346–349.

55 Kelly, K., Wang, S., Boddu, R., Liu, Z., Moukha-Chafiq, O., Augelli-Szafran, C. and West, A. B. (2018) The G2019S mutation in LRRK2 imparts resiliency to kinase inhibition. Exp. Neurol., Academic Press Inc. **309**, 1–13.

56 Casola, S. (2010) Mouse models for miRNA expression: the ROSA26 locus. Methods Mol. Biol. (Methods Protoc., Humana Press, Totowa, NJ **667**, 145–163.

57 Nichols, R. J., Dzamko, N., Morrice, N. A., Campbell, D. G., Deak, M., Ordureau, A., Macartney, T., Tong, Y., Shen, J., Prescott, A. R., et al. (2010) 14-3-3 Binding to LRRK2 is disrupted by multiple Parkinson's disease-associated mutations and regulates cytoplasmic localization. Biochem. J. **430**, 393–404.

58 Waschbüsch, D., Michels, H., Strassheim, S., Ossendorf, E., Kessler, D., Gloeckner, C. J. and Barnekow, A. (2014) LRRK2 transport is regulated by its novel interacting partner Rab32. PLoS One **9**.

59 Eguchi, T., Kuwahara, T., Sakurai, M., Komori, T., Fujimoto, T., Ito, G., Yoshimura, S. I., Harada,

A., Fukuda, M., Koike, M., et al. (2018) LRRK2 and its substrate Rab GTPases are sequentially targeted onto stressed lysosomes and maintain their homeostasis. Proc Natl Acad Sci U S A **115**, E9115–E9124.

60 Biskup, S., Moore, D. J., Celsi, F., Higashi, S., West, A. B., Andrabi, S. A., Kurkinen, K., Yu, S. W., Savitt, J. M., Waldvogel, H. J., et al. (2006) Localization of LRRK2 to membranous and vesicular structures in mammalian brain. Ann. Neurol. **60**, 557–569.

61 Kett, L. R., Boassa, D., Ho, C. C. Y., Rideout, H. J., Hu, J., Terada, M., Ellisman, M. and Dauer, W. T. (2012) LRRK2 Parkinson disease mutations enhance its microtubule association. Hum. Mol. Genet. **21**, 890–899.

62 Madero-Pérez, J., Fernández, B., Lara Ordóñez, A. J., Fdez, E., Lobbestael, E., Baekelandt, V. and Hilfiker, S. (2018) RAB7L1-mediated relocalization of LRRK2 to the golgi complex causes centrosomal deficits via RAB8A. Front. Mol. Neurosci. **11**, 1–19.

63 Bae, E. J., Kim, D. K., Kim, C., Mante, M., Adame, A., Rockenstein, E., Ulusoy, A., Klinkenberg, M., Jeong, G. R., Bae, J. R., et al. (2018) LRRK2 kinase regulates α-synuclein propagation via RAB35 phosphorylation. Nat. Commun., Springer US **9**.

64 Berndsen, K., Lis, P., Yeshaw, W. M., Wawro, P. S., Nirujogi, R. S., Wightman, M., Macartney, T., Dorward, M., Knebel, A., Tonelli, F., et al. (2019) PPM1H phosphatase counteracts LRRK2 signaling by selectively dephosphorylating rab proteins. Elife, eLife Sciences Publications Ltd **8**.

Figure Legends

Figure 1. Detection of endogenous Rab29 in human and mouse extracts with novel Rab29 monoclonal antibodies. (A) 30 μg of the indicated cell and tissue extracts were subjected to quantitative immunoblot analysis with the indicated antibodies, diluted to 1 μg/ml. The membranes were developed using the LI-COR Odyssey CLx Western Blot imaging system. **(B)** Various cell and tissue extracts were analyzed for Rab29 and LRRK2 expression (upper panels). Total protein levels were visualized using the Bio-Rad Oriole Fluorescent Gel Stain and exposed using the Bio-Rad Chemidoc MP Imaging System (lower panel). Total protein levels were quantified using Bio-Rad Image Lab software. Total Rab29 or total LRRK2 was quantified using the Image Studio software. Quantified data are presented as ratios of Rab29 or LRRK2 expression divided by total protein levels, and values were normalized to the average of the respective protein expression observed in MEFs. Quantifications are representative of three independent experiments and shown as mean ± SD.

Figure 2. Knock-out of Rab29 does not affect basal LRRK2 activity. (A) Two independent littermate-matched wildtype (WT), Rab29 knock-out heterozygous (+/-), or Rab29 knock-out homozygous (-/-) MEFs were treated with vehicle (DMSO) or 100 nM LRRK2 inhibitor MLi-2 for 90 min prior to harvest. 20 μg of whole cell extracts were subjected to quantitative immunoblot analysis with the indicated antibodies. Technical replicates represent cell extract obtained from a different dish of cells. The membranes were developed using the LI-COR Odyssey CLx Western Blot imaging system. Quantified data are presented as the mean ± SD of phospho-Rab10/total Rab10 and phospho-Rab12/total Rab12 ratios, which were quantified using the Image Studio software. Values were normalized to the average of Litter 1 wildtype MEFs treated with DMSO. Similar results were obtained in three independent experiments. **(B-D)** 6-month-old, littermate-matched wildtype (WT) and Rab29 knock-out (-/-) mice were administered with vehicle (40% (w/v) (2-hydroxypropyl)-β-cyclodextrin) or 30 mg/kg MLi-2 dissolved in vehicle by subcutaneous injection 2 hours prior to tissue collection. 40 μg of tissue extracts were analyzed by quantitative immunoblot as described in (A). Each lane represents tissue extract derived from a different mouse. Quantified data are presented as mean ± SD and values were normalized to the average of the wildtype, vehicle treated mice. Data were analyzed using two-tailed unpaired t-test and there was no statistical significance between WT and Rab29 knock-out mice. (B) lungs P-value = 0.6585 (C) spleen P-value = 0.9318 (D) kidneys P-value = 0.4793.

Figure 3. Characterization of MJFF transgenic Rab29 overexpressing mouse. (A) Schematic overview of design and targeting strategy utilized to create the Rab29 transgenic mouse model. The illustration depicts the transgene containing a neo cassette, a Pgk promoter, the murine Rab29 open reading frame together with a Kozak sequence (GCCACC), the human growth hormone polyadenylation signal and an additional polyadenylation signal. These elements were inserted into the ROSA26 locus via recombinase-mediated cassette exchange. **(B)** The indicated tissues were collected from 3.5-month-old and 6-month-old wildtype (WT) and homozygous, transgenic Rab29 overexpressing (Tg Rab29) mice. 30 μg of tissue extracts were subjected to quantitative immunoblot analysis with the indicated antibodies. The membranes were developed using the LI-COR Odyssey CLx Western Blot imaging system. Quantified data are presented as mean ± SD of total Rab29/GAPDH ratios, calculated using the Image Studio software. Values were normalized to the average of the

3.5-month-old wildtype mice. Each lane represents a tissue sample from a different animal. **(C)** The indicated tissue extracts from 3.5-month-old wildtype (WT), heterozygous (Tg Rab29 Het), and homozygous (Tg Rab29 Hom) transgenic Rab29 overexpressing mice were processed for total RNA extraction, cDNA synthesis, and subsequent quantitative real time RT-PCR analysis. Rab29 mRNA levels were normalized to β-Actin mRNA levels and further normalized to wildtype of the appropriate tissue. Quantified data are presented as mean ± SD of four biological replicates per genotype.

Figure 4. Overexpression of Rab29 does not impact LRRK2-mediated Rab10 phosphorylation. **(A-F)** 6-month-old littermate-matched wildtype (WT) and homozygous, transgenic Rab29 overexpressing (Tg Rab29 Hom) mice were administered with vehicle (40% (w/v) (2-hydroxypropyl)-β-cyclodextrin) or 30 mg/kg MLi-2 dissolved in vehicle by subcutaneous injection 2 hours prior to tissue collection. 40 μg of tissue extracts were subjected to quantitative immunoblot analysis with the indicated antibodies. The membranes were developed using the LI-COR Odyssey CLx Western Blot imaging system. Quantified data are presented as the ratios of phospho-Rab10/total Rab10, calculated using the Image Studio software. Values were normalized to the average of the wildtype, vehicle treated mice. Each lane represents a tissue sample from a different animal. Quantifications are presented as mean ± SD and data were analyzed using two-tailed unpaired t-test. There was no statistical significance between wildtype and homozygous, transgenic Rab29 overexpressing mice. The resulting P-values from the aforementioned statistical analyses are as follows: (A) brain P= 0.0625 (B) large intestine P = 0.8026 (C) kidneys P = 0.7243 (D) lungs P = 0.1676 (E) spleen P = 0.7257 (F) spinal cord P = 0.3120.

Figure 5. Knock-out of Rab29 does not reduce elevated Rab10 phosphorylation in pathogenic LRRK2[R1441C] knock-in mice. (A) The indicated matched primary MEFs were treated with vehicle (DMSO) or 100 nM LRRK2 inhibitor MLi-2 for 90 min prior to harvest. 20 μg of whole cell extracts were subjected to quantitative immunoblot analysis with the indicated antibodies. Technical replicates represent cell extract obtained from a different dish of cells. Cell extract derived from a wildtype MEF cell line (WT*) was added to each gel in order to accurately compare the Rab10 pThr73/Rab10 total ratios between genotypes. The membranes were developed using the LI-COR Odyssey CLx Western Blot imaging system. Quantified data are presented as the ratios of phospho-Rab10/total Rab10, calculated using the Image Studio software. Values were normalized to the average of wildtype MEFs treated with DMSO. Similar results were obtained in two separate experiments. Quantifications are presented as mean ± SD. Data were analyzed by one-way ANOVA with Tukey's multiple comparison test and there was a statistically significant difference between wildtype and LRRK2[R1441C] knock-in MEFs (****P < 0.0001) but not between wildtype and Rab29 knock-out MEFs (P-value 0.8351) or between LRRK2[R1441C] knock-in and Rab29 knock-out LRRK2[R1441C] knock-in MEFs (P-value 0.9452). **(B-D)** The indicated 6-month-old matched mice were administered with vehicle (40% (w/v) (2-hydroxypropyl)-β-cyclodextrin) or 30 mg/kg MLi-2 dissolved in vehicle by subcutaneous injection 2 hours prior to tissue collection. 40 μg of tissue extracts were subjected to quantitative immunoblot analysis with the indicated antibodies. The membranes were developed using the LI-COR Odyssey CLx Western Blot imaging system. Quantified data are presented as the ratios of phospho-Rab10/total Rab10, which were calculated using the Image Studio software. Quantifications are presented as mean ± SD, normalized to vehicle

treated, wildtype animals. Each lane represents a tissue sample from a different animal. Data was analyzed by one-way ANOVA with Tukey's multiple comparison test and there was a statistically significant difference between wildtype and LRRK2[R1441C] spleen samples (**P = 0.0093 (D)). All other comparisons were not statistically significant. Wildtype vs LRRK2[R1441C]: P = 0.2792 (B), P = 0.1555 (C). Wildtype vs Rab29 knock-out: P = 0.8942 (B), P = 0.9372 (C), P = 0.3964 (D). LRRK2[R1441C] vs Rab29 knock-out LRRK2[R1441C]: P = 0.9955 (B), P = 0.9962 (C), P = 0.4184 (D).

Figure 6. Rab29 knock-out does not reduce the enhanced LRRK2-mediated phosphorylation of Rab10 in VPS35[D620N] knock-in mice. (A) The indicated matched MEFs were treated with vehicle (DMSO) or 100 nM LRRK2 inhibitor MLi-2 for 90 min prior to harvest. 15 μg of whole cell extracts were subjected to quantitative immunoblot analysis with the indicated antibodies. Technical replicates represent cell extract obtained from a different dish of cells. Cell extract derived from a wildtype MEF cell line (WT*) was added to each gel in order to accurately compare the Rab10 pThr73/Rab10 total ratios between genotypes. The membranes were developed using the LI-COR Odyssey CLx Western Blot imaging system. Quantified data are presented as the ratios of phospho-Rab10/total Rab10, calculated using the Image Studio software. Values were normalized to the average of wildtype MEFs treated with DMSO. Similar results were obtained in two separate experiments. Quantifications are presented as mean ± SD. Data were analyzed by one-way ANOVA with Tukey's multiple comparison test and there was a statistically significant difference between wildtype and VPS35[D620N] knock-in MEFs (****P < 0.0001) but not between wildtype and Rab29 knock-out MEFs (P-value = 0.9792) or between VPS35[D620N] knock-in and Rab29 knock-out VPS35[D620N] knock-in MEFs (P-value = 0.6952). **(B-D)** The indicated 6-month-old matched mice were administered with vehicle (40% (w/v) (2-hydroxypropyl)-β-cyclodextrin) or 30 mg/kg MLi-2 dissolved in vehicle by subcutaneous injection 2 hours prior to tissue collection. 40 μg of tissue extracts were subjected to quantitative immunoblot analysis with the indicated antibodies. The membranes were developed using the LI-COR Odyssey CLx Western Blot imaging system. Quantified data are presented as the ratios of phospho-Rab10/total Rab10, calculated using the Image Studio software. Quantifications are presented as mean ± SD, normalized to vehicle treated, wildtype animals. Each lane represents a tissue sample from a different animal. Data were analyzed by one-way ANOVA with Tukey's multiple comparison test and there was a statistically significant difference between wildtype and VPS35[D620N] samples (Lungs **P = 0.0094 (B), Kidneys ****P < 0.0001 (C), Spleen ***P = 0.0001 (D)). All other comparisons were not statistically significant. Wildtype vs Rab29 knock-out: P = 0.9270 (B), P = 0.7648 (C), P = 0.1233 (D). VPS35[D620N] vs Rab29 knock-out VPS35[D620N]: P = 0.5654 (B), P = 0.1329 (C), P = 0.5075 (D).

Figure 7. Rab29 knock-out does not impact recovery of LRRK2 activity following washout of LRRK2 inhibitor. (A-C) The indicated matched MEFs were treated with vehicle (DMSO) or 100 nM LRRK2 inhibitor MLi-2 for 48 hours. The MLi-2 inhibitor was removed from cells through multiple washes with complete media for the indicated periods prior to cell lysis. 20 μg of whole cell extracts were subjected to quantitative immunoblot analysis with the indicated antibodies. The membranes were developed using the LI-COR Odyssey CLx Western Blot imaging system. Quantified data are presented as the ratios of phospho-Rab10/Total Rab10, which were calculated using the Image Studio software. Values were

normalized to the average of **(A)** wildtype MEFs treated with DMSO, **(B)** LRRK2[R1441C] MEFs treated with DMSO, or **(C)** VPS35[D620N] MEFs treated with DMSO. Cell extract derived from a wildtype MEF cell line (**) was added to each gel in order to accurately compare the Rab10 pThr73/Rab10 total ratios between genotypes in each panel. Data quantifications are presented as mean ± SD. Similar results were obtained in two separate experiments.

Figure 8. Knockdown of Rab32 does not impact LRRK2 activity in the absence of Rab29. The indicated matched primary MEFs were transfected with Dharmacon smartPOOL siRNA targeting either LRRK2, Rab32, or control scrambled non-targeting siRNA. The cells were lysed 72 hours post-transfection. 20 μg of whole cell extracts were subjected to quantitative immunoblot analysis with the indicated antibodies. The membranes were developed using the LI-COR Odyssey CLx Western Blot imaging system. Quantified data are presented as the ratios of phospho-Rab10/Total Rab10 and were calculated using the Image Studio software. Values were normalized to the average of Rab29 knock-out MEFs treated with scrambled siRNA. The ratio of LRRK2 or Rab32 expression divided by Tubulin was used to determine siRNA knockdown efficiency, and values were normalized to the average of the scrambled siRNA treated MEFs. Data quantifications are represented as mean ± SD. Similar results were obtained in three separate experiments.

Supplementary Figure 1. Knock-out of Rab29 does not affect LRRK2 Ser935 phosphorylation or LRRK2-mediated Rab10 phosphorylation in brain. (A) As in Figure 2 (B-D), 6-month-old, littermate-matched wildtype (WT) and Rab29 knock-out (-/-) mice were administered with vehicle (40% (w/v) (2-hydroxypropyl)-β-cyclodextrin) or 30 mg/kg MLi-2 dissolved in vehicle by subcutaneous injection 2 hours prior to tissue collection. 40 μg of tissue extracts derived from 7 different brain sections were analyzed by quantitative immunoblot with the indicated antibodies. Each lane represents tissue extract derived from a different mouse. **(B)** Quantified data are presented as the mean ± SD of phospho-Rab10/Total Rab10 ratios and phospho-LRRK2/total LRRK2 ratios, and values were quantified using the Image Studio software.

Supplementary Figure 2. Overexpression of Rab29 in tissues from 3.5-month-old mice does not impact LRRK2-mediated Rab10 phosphorylation. **(A-E)** 3.5-month-old wildtype (WT), heterozygous (Tg Rab29 Het), and homozygous (Tg Rab29 Hom), transgenic Rab29 overexpressing mice were administered with vehicle (40% (w/v) (2-hydroxypropyl)-β-cyclodextrin) or 30 mg/kg MLi-2 dissolved in vehicle by subcutaneous injection 2 hours prior to tissue collection. 40 μg of tissue extracts were subjected to quantitative immunoblot analysis with the indicated antibodies. The membranes were developed using the LI-COR Odyssey CLx Western Blot imaging system. Quantified data are presented as the phospho-Rab10/GAPDH ratios calculated using the Image Studio software. Values were normalized to the average of the wildtype, vehicle treated mice. Each lane represents a tissue sample derived from a different animal. Quantifications are presented as mean ± SD.

Supplementary Figure 3. Overexpression of Rab29 in MEFs or primary lung fibroblasts does not impact LRRK2-mediated Rab10 phosphorylation. **(A)** Littermate-matched wildtype (WT), heterozygous (Tg Rab29 Het), or homozygous (Tg Rab29 Hom), transgenic Rab29 overexpressing MEFs were treated with vehicle (DMSO) or 100 nM LRRK2 inhibitor MLi-2 for 90 min prior to harvest. 20 μg of whole cell extracts were subjected to quantitative immunoblot analysis with the indicated antibodies. Technical replicates represent cell extract obtained from a different dish of cells. The membranes were developed using the LI-COR Odyssey CLx Western Blot imaging system. Quantified data are presented as the mean ± SD of phospho-Rab10/total Rab10 and phospho-Rab12/total Rab12. Rab29 levels were quantified by calculating the ratio of total Rab29/GAPDH. Data quantifications were undertaken using the Image Studio software and values were normalized to the average of wildtype MEFs treated with DMSO. **(B)** Primary lung fibroblasts derived from 3 different wildtype (WT) mice and 2 different transgenic, homozygous Rab29 overexpressing (Tg Rab29 Hom) mice were treated with vehicle (DMSO) or 100 nM LRRK2 inhibitor MLi-2 for 90 min prior to harvest. 20 μg of whole cell extracts were subjected to quantitative immunoblot analysis with the indicated antibodies. Technical replicates represent cell extract obtained from a different dish of cells. Quantified data are presented as the mean ± SD of phospho-Rab10/total Rab10. Rab29 levels were quantified by the ratio of total Rab29/GAPDH. Data quantifications were undertaken using the Image Studio software and values were normalized to the average of wildtype primary lung fibroblasts treated with DMSO.

Supplementary Figure 4. Knock-out of Rab29 does not reduce elevated Rab10 phosphorylation in pathogenic LRRK2[R1441C] knock-in mice. (A-C) As in Figure 5 (B-D), the indicated 6-month-old matched mice were administered with vehicle (40% (w/v) (2-hydroxypropyl)-β-cyclodextrin) or 30 mg/kg MLi-2 dissolved in vehicle by subcutaneous injection 2 hours prior to tissue collection. 40 μg of tissue extracts were subjected to quantitative immunoblot analysis with the indicated antibodies. The membranes were developed using the LI-COR Odyssey CLx Western Blot imaging system. Quantified data are presented as the ratios of phospho-Rab10/total Rab10, calculated with the Image Studio software. Quantifications are presented as mean ± SD, normalized to vehicle treated, wildtype animals. Each lane represents a tissue sample from a different animal. Data were analyzed by one-way ANOVA with Tukey's multiple comparison test and no statistical significance was determined between the genotypes. Wildtype vs LRRK2[R1441C]: P = 0.1413 (A), P = 0.7169 (B), P = 0.7459 (C). Wildtype vs Rab29 knock-out: P = 0.9455 (A), P = 0.2594 (B), P = 0.7867 (C). LRRK2[R1441C] vs Rab29 knock-out LRRK2[R1441C]: P = 0.9973 (A), P = 0.6629 (B), P = 0.9768 (C).

Supplementary Figure 5. Rab29 knock-out does not reduce the enhanced LRRK2-mediated phosphorylation of Rab10 in VPS35[D620N] knock-in mice. (A-C) As in Figure 6 (B-D), the indicated 6-month-old matched mice were administered with vehicle (40% (w/v) (2-hydroxypropyl)-β-cyclodextrin) or 30 mg/kg MLi-2 dissolved in vehicle by subcutaneous injection 2 hours prior to tissue collection. 40 μg of tissue extracts were subjected to quantitative immunoblot analysis with the indicated antibodies. The membranes were developed using the LI-COR Odyssey CLx Western Blot imaging system. Quantified data are presented as the ratios of phospho-Rab10/total Rab10, calculated using the Image Studio software. Quantifications are presented as mean ± SD, normalized to vehicle treated,

wildtype animals. Each lane represents a tissue sample from a different animal. Data were analyzed by one-way ANOVA with Tukey's multiple comparison test and there was a statistically significant difference between wildtype and VPS35[D620N] large intestine samples (**P = 0.0072 (A)), but not between wildtype and VPS35[D620N] brain (P = 0.0738 (B)) or spinal cord (P = 0.8768 (C)). All other comparisons were not statistically significant. Wildtype vs Rab29 knock-out: P = 0.9092 (A), P = 0.6120 (B), P = 0.8629 (C). VPS35[D620N] vs Rab29 knock-out VPS35[D620N]: P = 0.6516 (A), P = 0.6015 (B), 0.3935 (C).

Table 1. Antigens used in the MJFF rabbit monoclonal Rab29 program

ABCAM Project Number	Antigen
MJF-30	Recombinant full-length Rab29 (residues 1-203, human) N-terminal Rab29 peptide (Ac-MGSRDHLFKVLVVGDAAVGK-Ahx-C residues 1 to 20 of human Rab29) C-terminal Rab29 peptide (Ac-RNSTEDIMSLSTQGDYINLQTKSSSWS-Ahx-C, residues 174 to 201 of human Rab29)

Table 2. Summary of mouse models used in this study

Name of model	Strain designation	Provider	Previously characterized
Rab29 knock-out	Rab29$^{tm1a(EUCOMM)Wtsi}$/WtsiOulu	Wellcome Sanger Institute, Infrafrontier EMMA mouse repository EM: 05517	(Kuwahara *et al.*, 2016; Beilina *et al.*, 2020; Mazza *et al.*, 2020)
LRRK2[R1441C]	B6.Cg-Lrrk2$^{tm1.1Shn}$/J	Jackson Laboratories Stock No: 009346	(Steger *et al.*, 2017; Lis *et al.*, 2018)
VPS35[D620N]	B6(Cg)-Vps35$^{tm1.1Mjff}$/J	Jackson Laboratories Stock No: 023409	(Mir *et al.*, 2018)
Transgenic Rab29 overexpression	C57BL/6NTac-*Gt(ROSA)26Sor*$^{tm1(Pgk-Rab29)Tac}$	Taconic Model No: 16552	

Figure 1

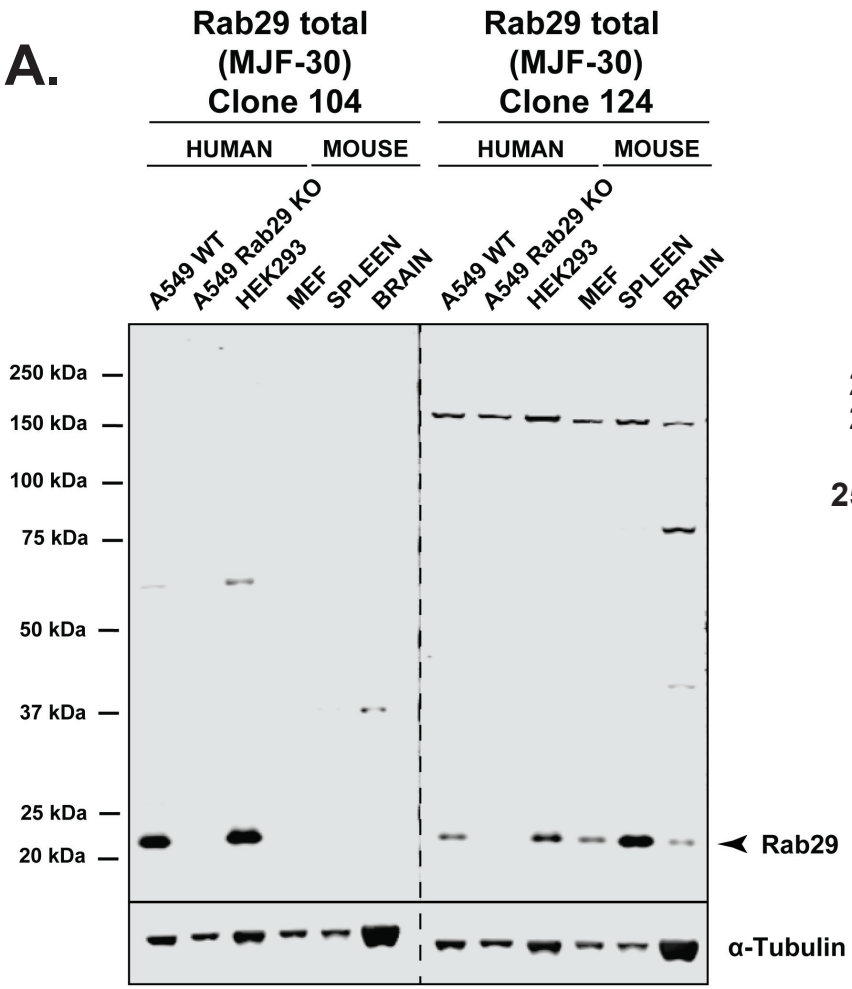

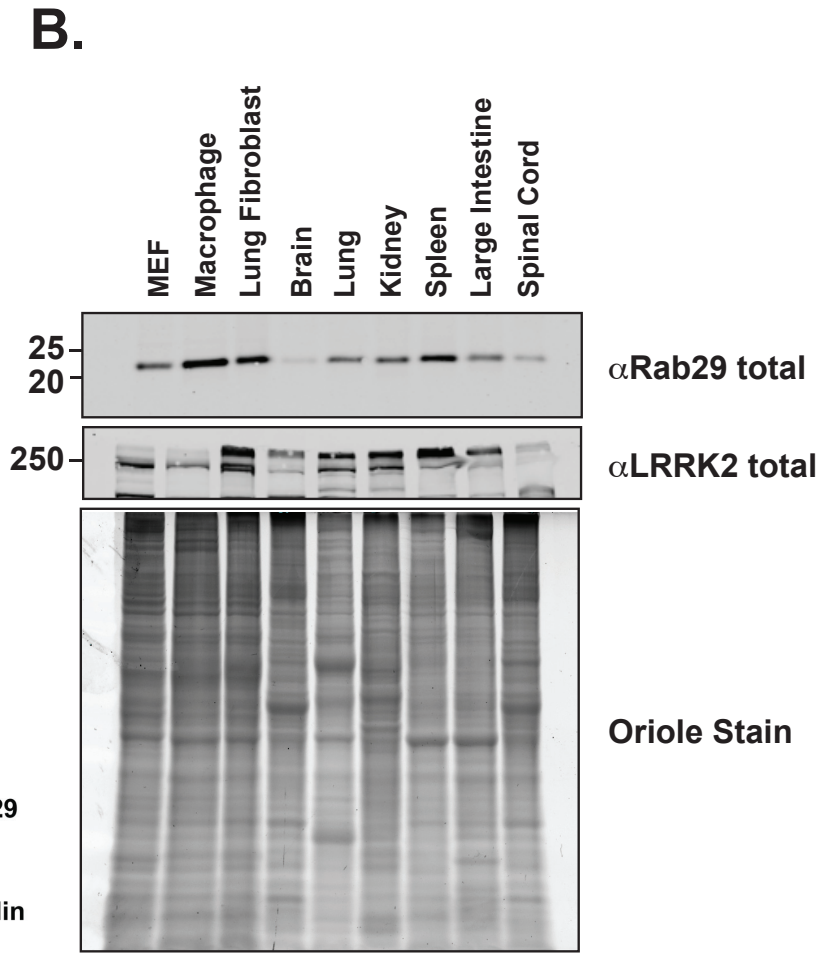

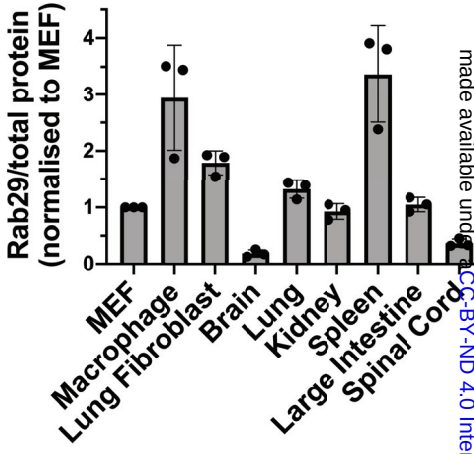

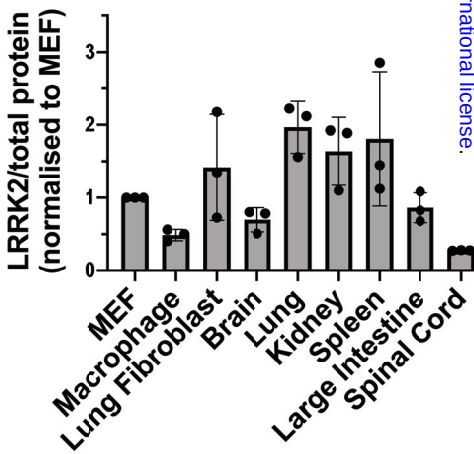

Figure 2

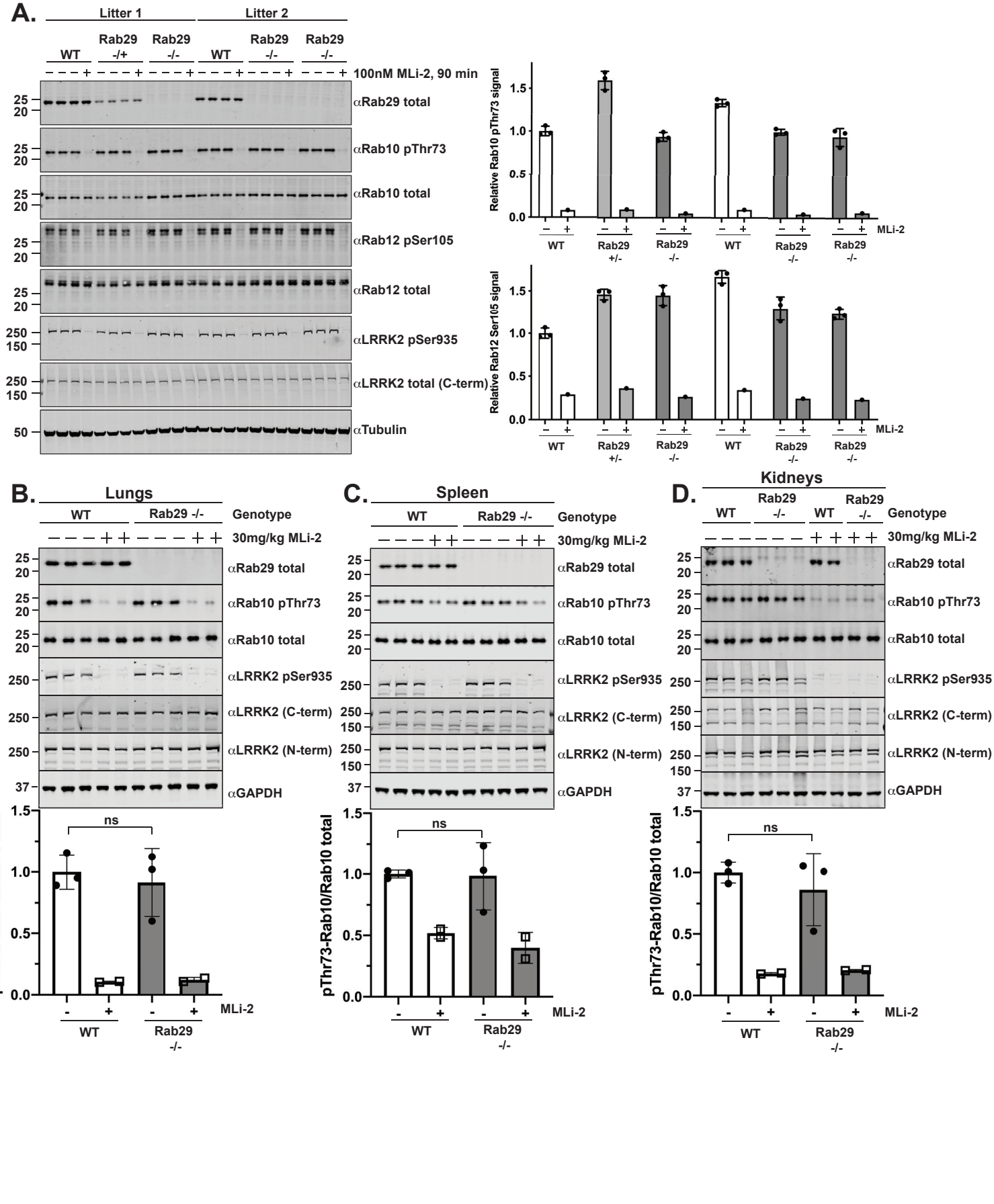

Figure 3

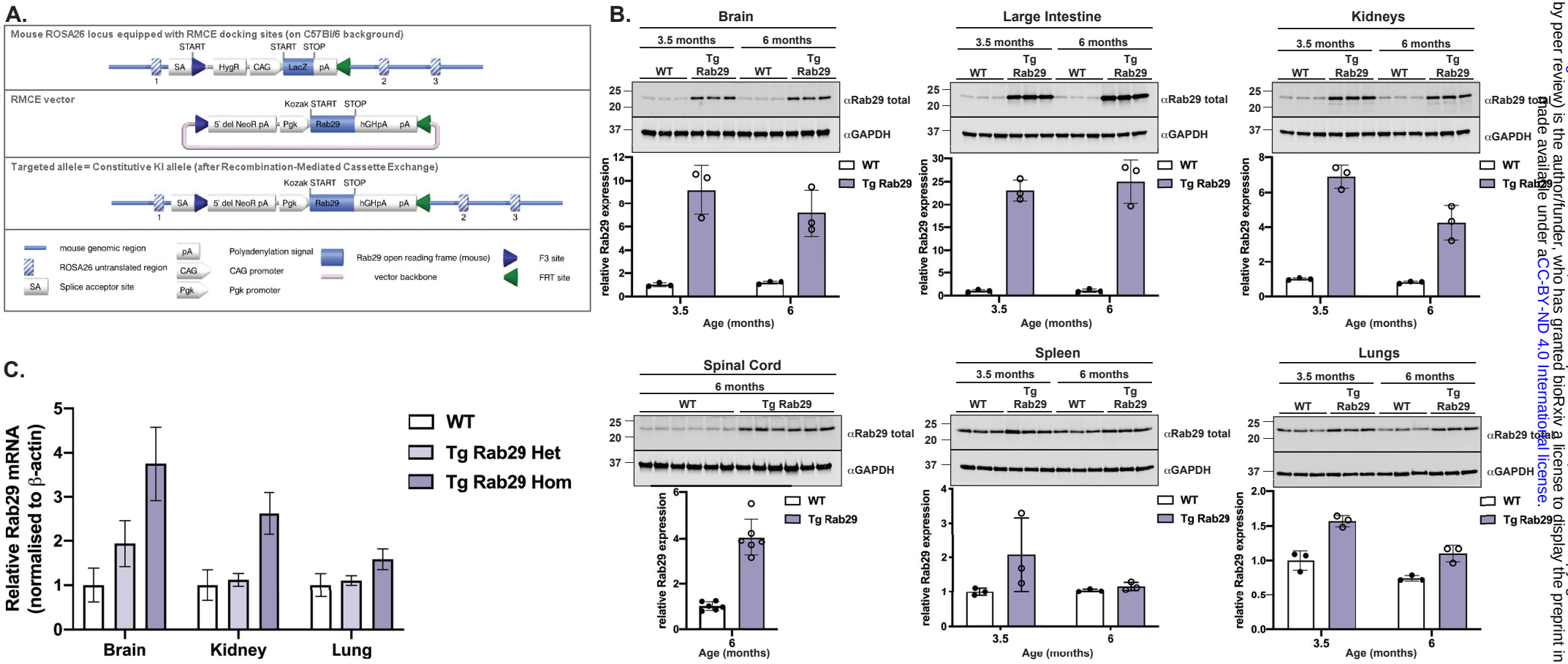

Figure 4

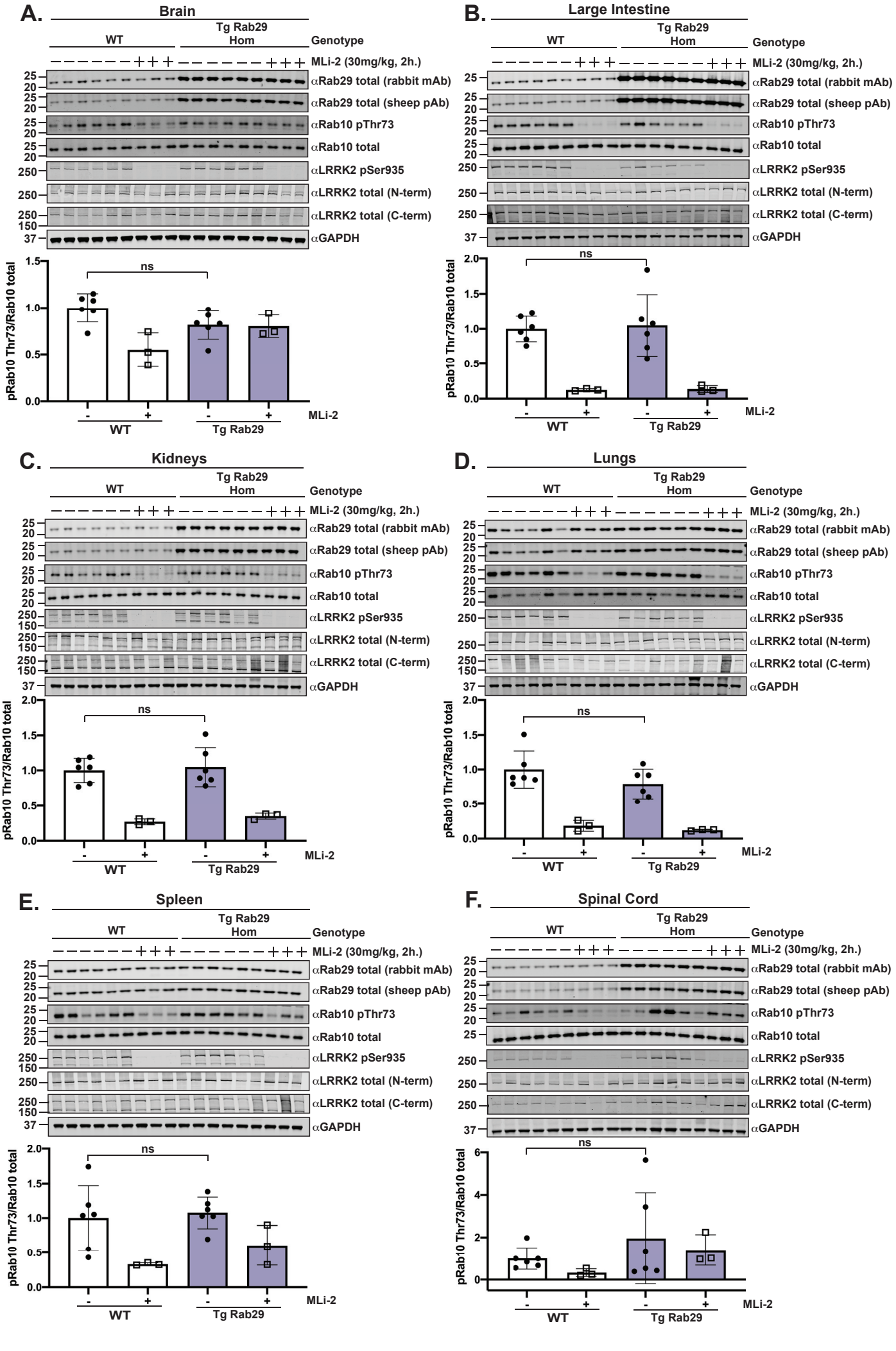

Figure 5

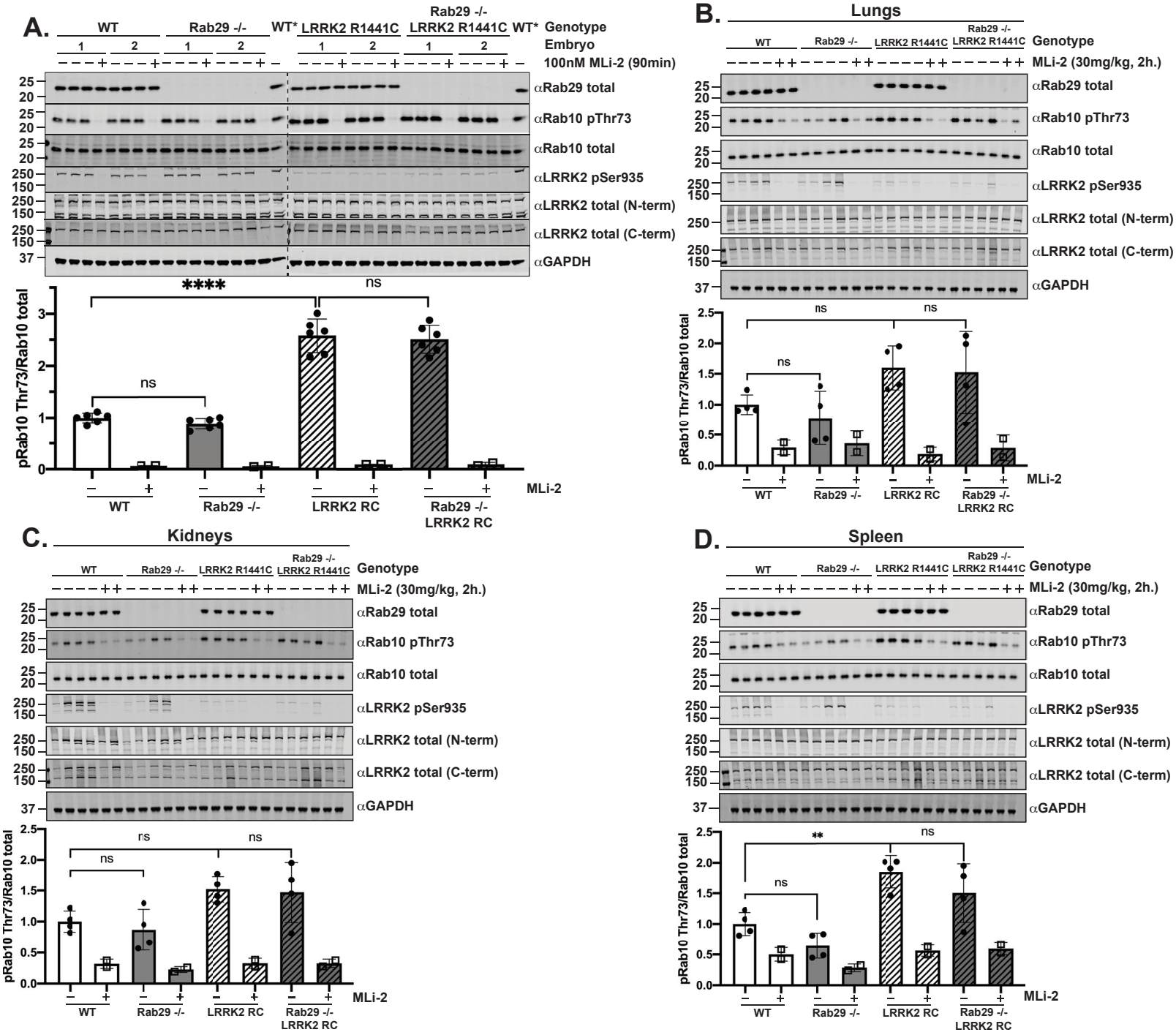

Figure 6

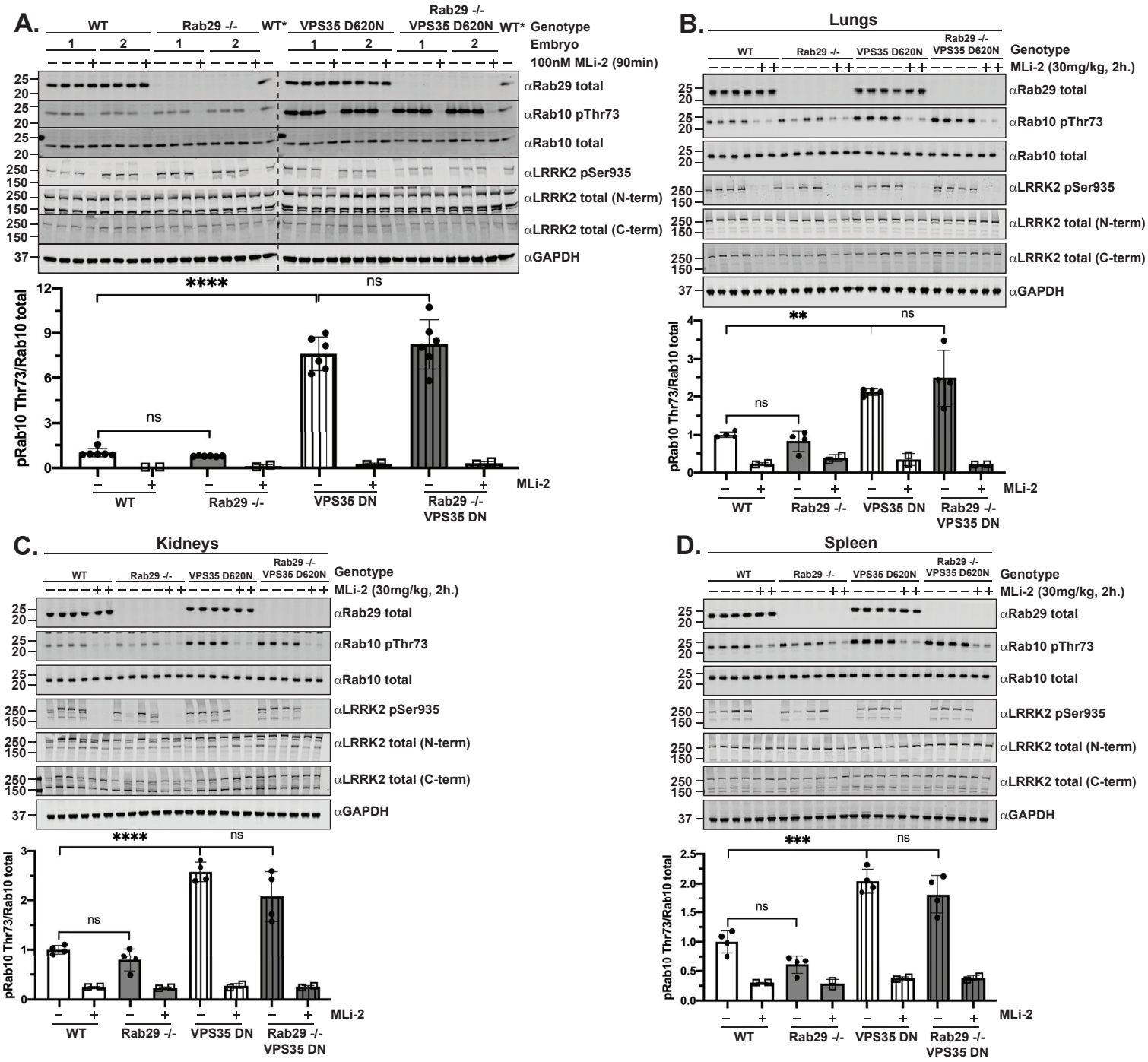

Figure 7

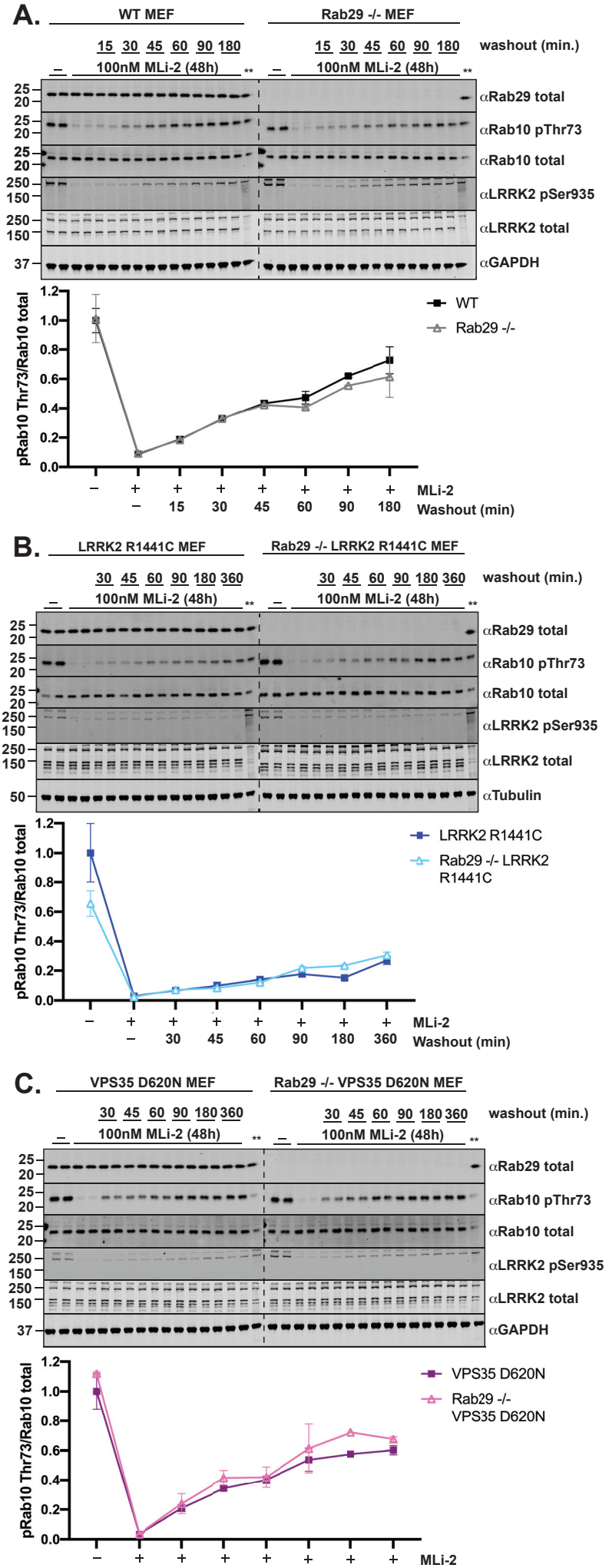

Figure 8

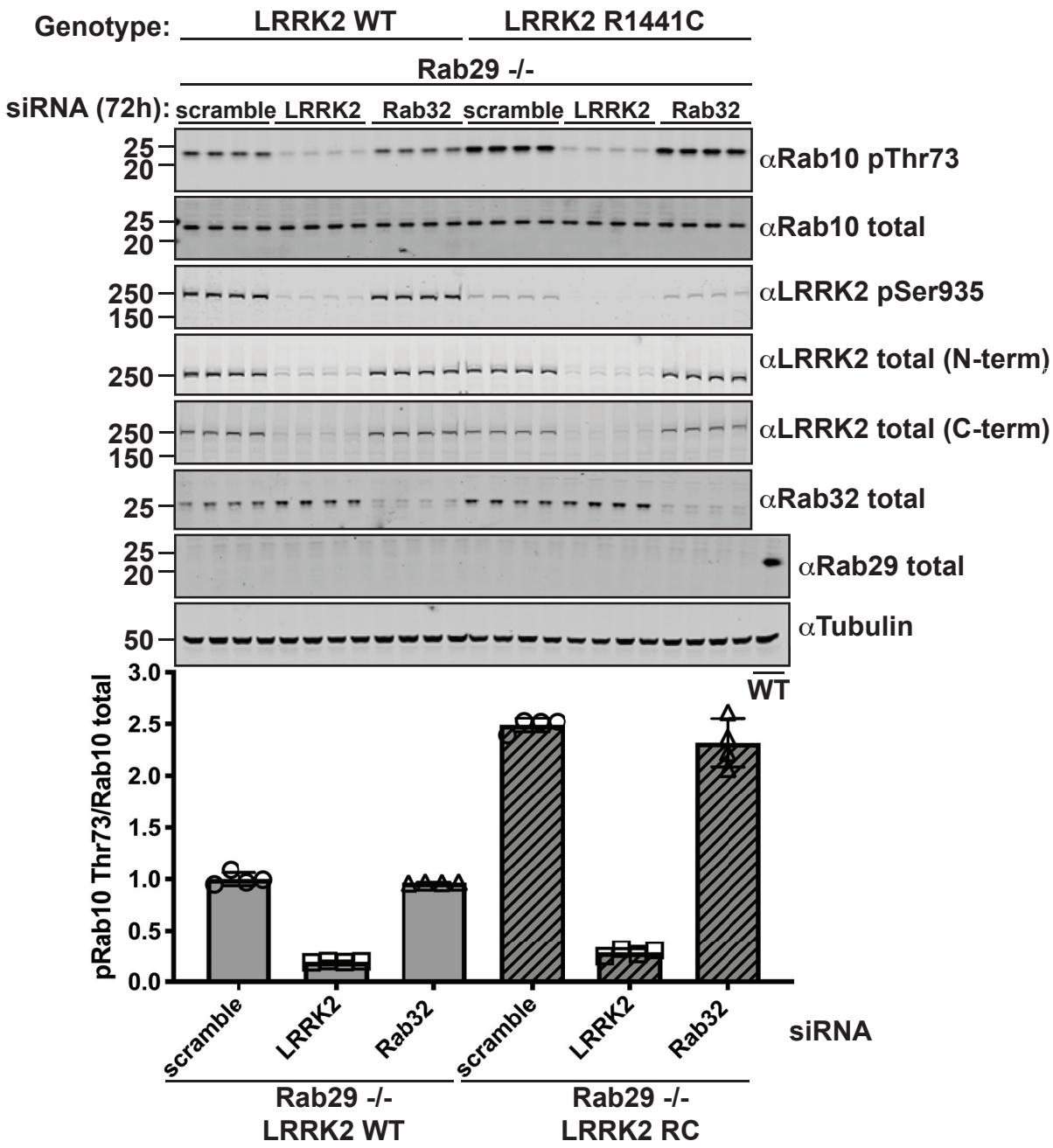

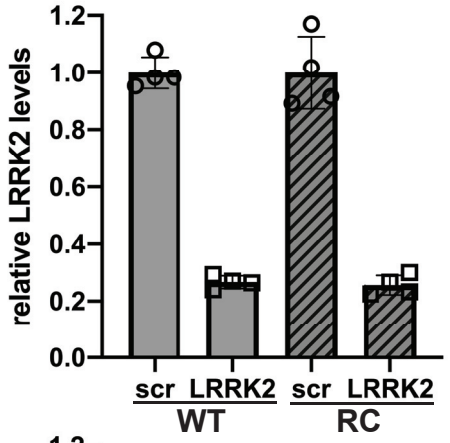

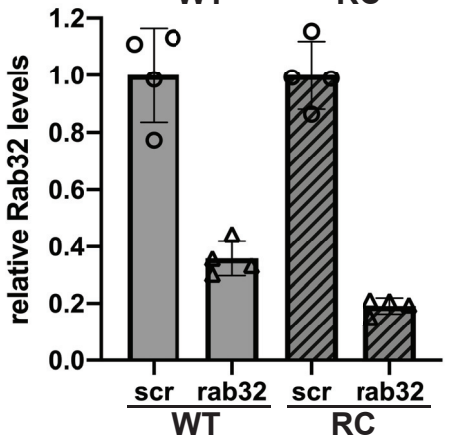

Supplementary Figure 1

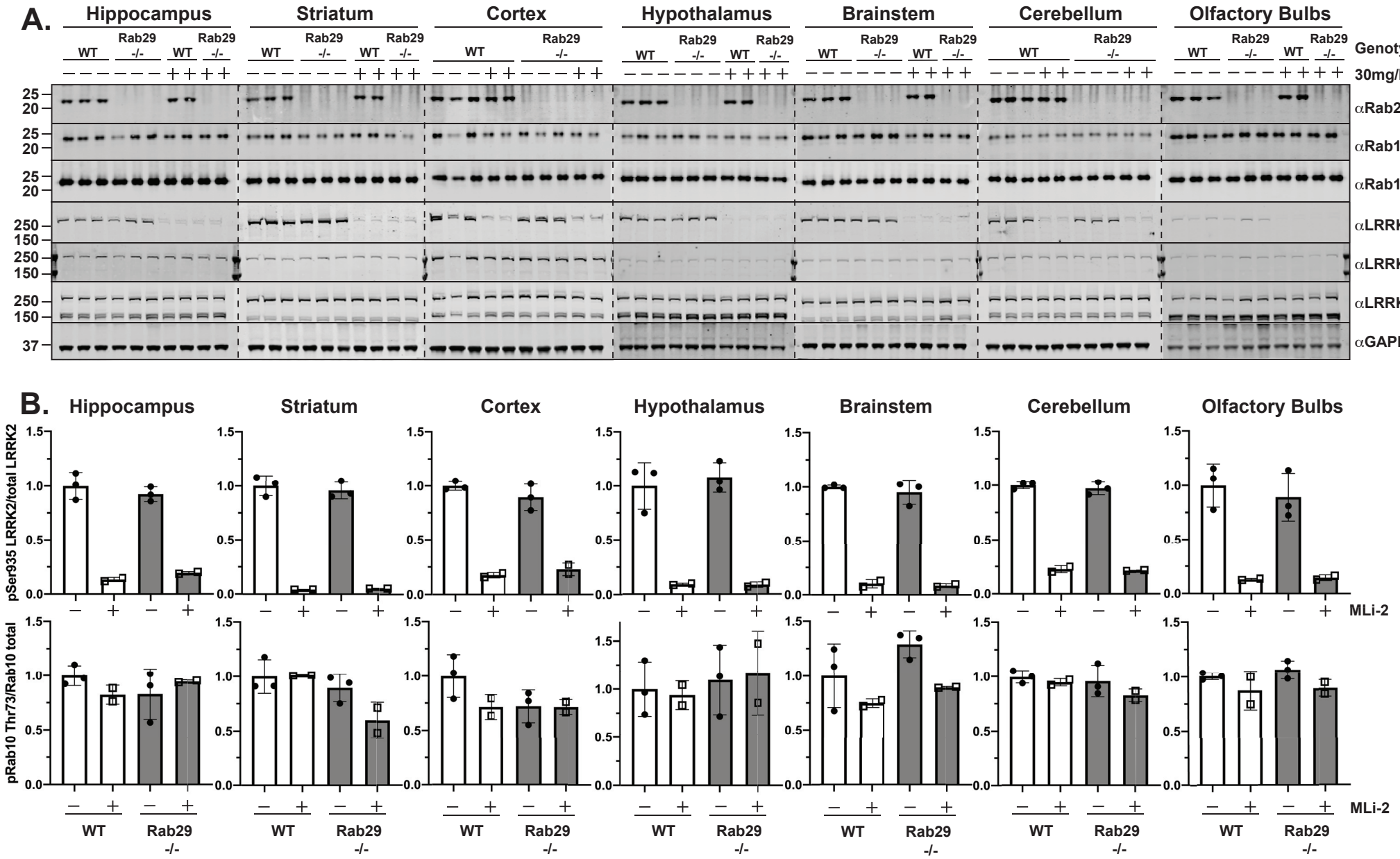

Supplementary Figure 2

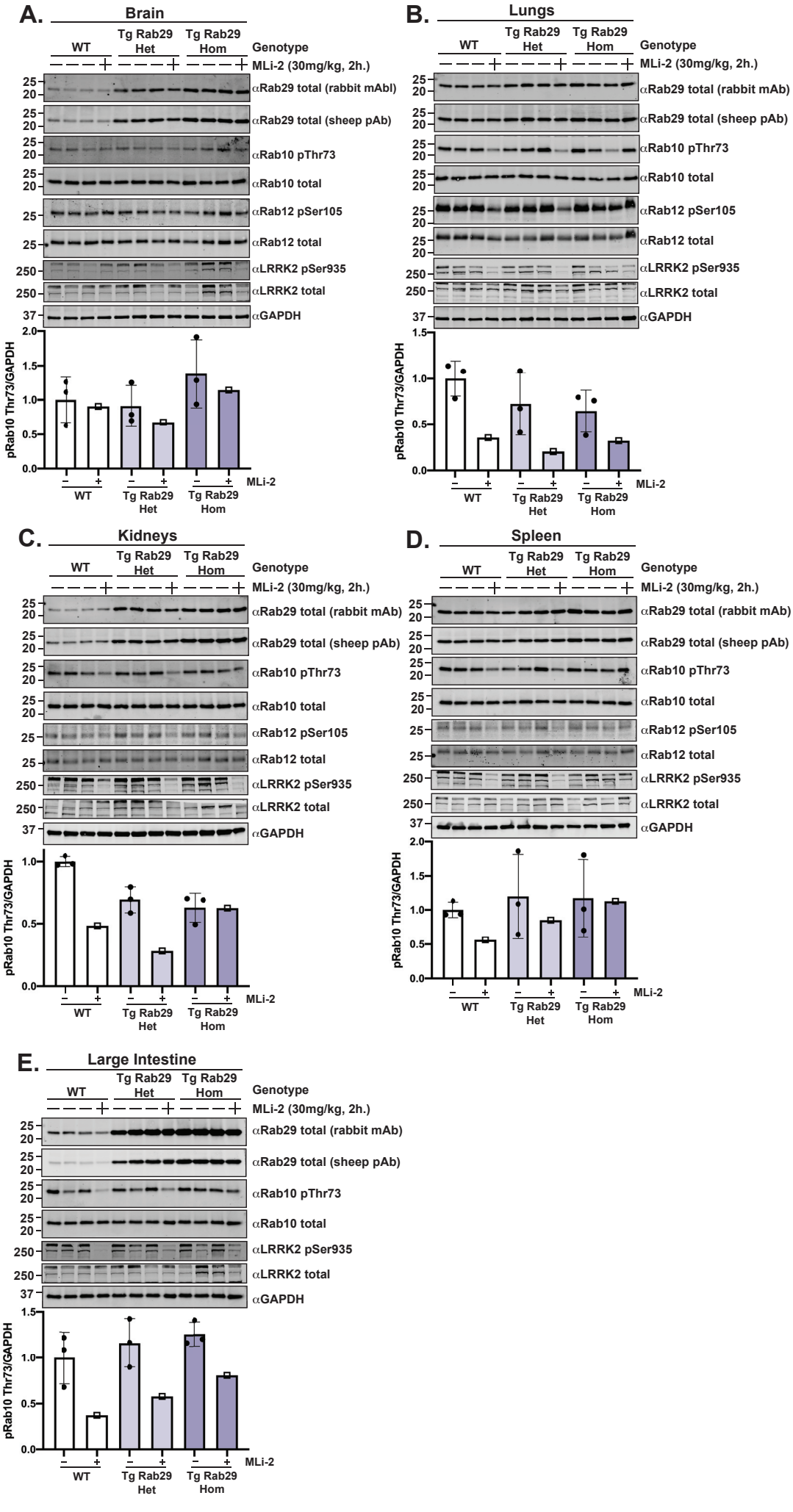

Supplementary Figure 3

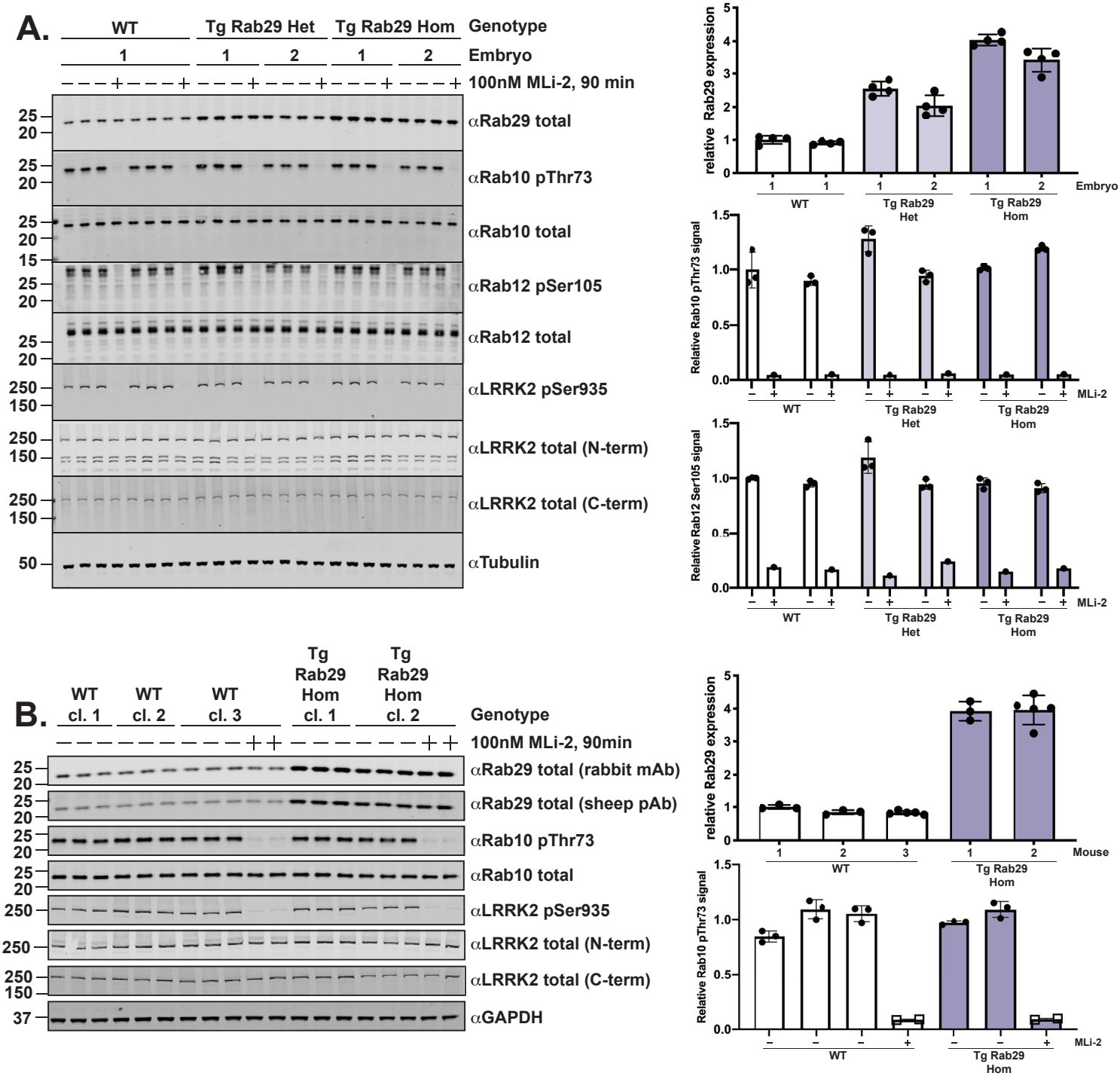

Supplementary Figure 4

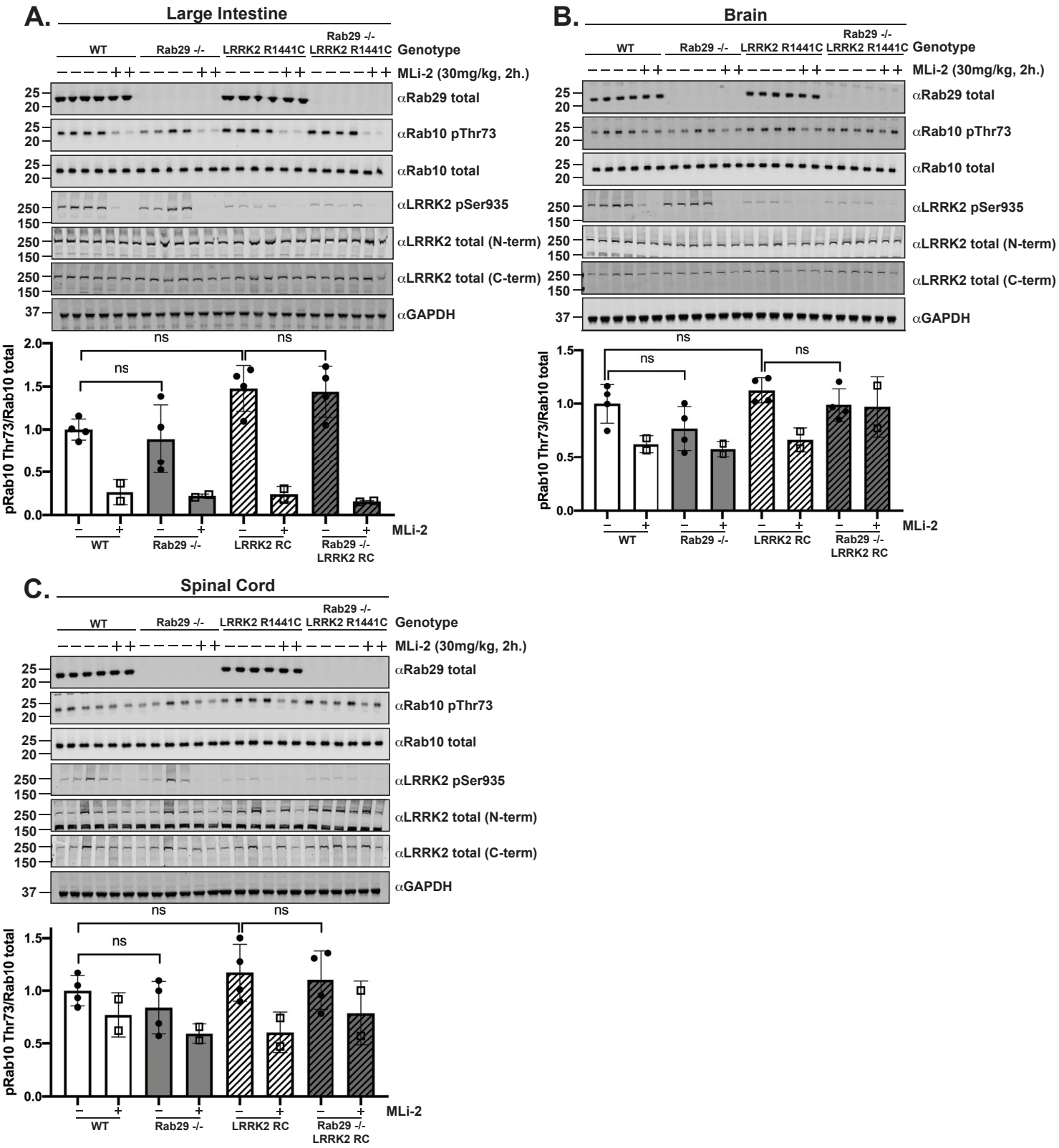

Supplementary Figure 5